Collective Excitations and Optical Response of Ultrathin Carbon-Nanotube Films

Igor V. Bondarev* and Chandra M. Adhikari
Department of Mathematics & Physics, North Carolina Central University, Durham, North Carolina 27707, USA

(Received 25 November 2020; accepted 25 January 2021; published 1 March 2021)

We present a theoretical study of the collective quasiparticle excitations responsible for the electromagnetic response of ultrathin plane-parallel homogeneous periodic single-wall carbon-nanotube arrays and weakly inhomogeneous single-wall carbon-nanotube films. We show that in addition to varying film composition, the collective response can be controlled by varying the film thickness. For single-type nanotube arrays, the real part of the dielectric response shows a broad negative refraction band near a quantum interband transition of the constituent nanotube, whereby the system behaves as a hyperbolic metamaterial at higher frequencies than those classical plasma oscillations have to offer. By decreasing nanotube diameters it is possible to push this negative refraction into the visible region, and using weakly inhomogeneous multitype nanotube films broadens its bandwidth.

DOI: 10.1103/PhysRevApplied.15.034001

I. INTRODUCTION

In recent years, optical nanomaterials research has uncovered the intriguing capabilities of carbon nanotubes (CNs). These hollow graphene cylinders of one to a few nanometers in diameter and up to one centimeter in length [1–3] have landed themselves to attractive device applications [4–14]. CNs have been successfully integrated into miniaturized electronic, electromechanical, and chemical devices [15–19]. The strong potential of CNs has been demonstrated in the fields of optical absorption and scattering spectroscopy [20–24], electron energy-loss spectroscopy [25,26], quantum electron transport [5,14,27], and general collective electromagnetic (EM) response phenomena [28–43]. Carbon-nanotube-based reduced-dimensionality materials such as periodic and quasiperiodic plane-parallel CN arrays and films, offer extraordinary stability, flexibility, and precise tunability of their physical properties by varying the density, diameter, and chirality of constituent CNs. Thin and ultrathin periodically aligned arrays of single-wall CNs (SWCNs) and related systems are currently in the process of rapid experimental development [44–54].

In this paper, we develop a theory for collective near-field interactions and associated EM response of ultrathin, closely packed, periodically aligned SWCN arrays (schematic shown in Fig. 1). The key features that make this system interesting for theoretical study are the periodic CN alignment and the spatially periodic anisotropy associated with it. Additionally, the vertical confinement in dense ultrathin planar systems of finite thickness leads to the effective dimensionality reduction from three dimensional (3D) to two dimensional (2D) while still retaining the thickness as a parameter to represent the vertical size [55–58]. This is the transdimensional (TD) regime [59]—neither 3D nor 2D but something in between—turning into 2D as thickness tends to zero, challenging to study what the 3D-to-2D continuous transition has to offer to improve material functionalities.

The spatial anisotropy, periodic in-plane transverse inhomogeneity and vertical quantum confinement make the ultrathin array near fields strong and anisotropically nonlocal, adding both extra challenges in developing the problem theoretically and extra flexibility in designing CN films with desired EM properties experimentally. The properties of the CN array can be controlled if one knows how to control its collective excitations such as excitons, plasmons, and their mutual interactions. For example, plasmon generated near fields are known to affect spontaneous emission [39,60], low-energy absorption [20], and scattering [24] by atomic type species near the CN surface. CN periodicity allows for the formation of plasmonic bands [61–63], whereby periodic CN arrays and films should behave as epsilon-near-zero plasmonic metamaterials (MMs) in the near field, while still remaining strong light absorbers and polarizers in the far field [51,64]. Indeed, recent ellipsometry measurements on finite-thickness films of horizontally aligned self-assembled SWCNs have exhibited their tunable negative dielectric response for a sufficiently wide range of the photon excitation energies [51,52], thus paving the way for the highly anisotropic hyperbolic MM (HMMs) film (metasurface) development. HMMs and metasurfaces (MSs) can be used in a variety of applications [65–68] such

*ibondarev@nccu.edu

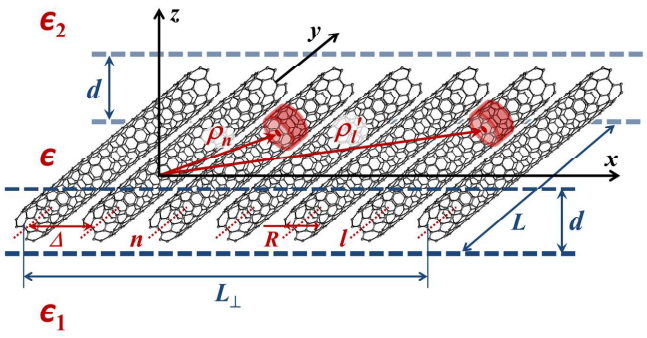

FIG. 1. Schematic of a plane-parallel, closely packed, periodically aligned array of SWCNs of radius R and length L embedded in a dielectric of thickness d. See text for details.

as optical sensing [69], absorption [70], cloaking [71], and super-resolution imaging [72]. Being very stable and highly sensitive to the thickness, CN density, diameter and chirality variation, the finite-thickness parallel aligned SWCN arrays and films can additionally serve as a flexible multifunctional nanomaterial platform for single-molecule detection and manipulation [73–75], including the near-field control of photoluminescence rate and directionality [39,60], chemical reactivity [76,77], and Casimir-Polder interactions [78,79].

In this paper, we formulate the general Hamiltonian for the collective quasiparticle excitations in the ultrathin plane-parallel periodic SWCN array in the TD regime. This Hamiltonian is used to derive the in-plane dynamical dielectric response tensor of the system in the broadband low-energy spectral range of microwave to visible ($\lesssim 1-2$ eV). This is the domain where the intrinsic excitations, excitons and plasmons, are present in individual constituent (metallic and semiconducting) CNs [24,29]. As opposed to the earlier 3D effective-medium response theories (known to be of limited validity at short CN separations) with only one single-tube excitation taken into account (the 6-eV bulk graphite plasmon) [61–63], our approach starts with the single-tube dynamical surface-conductivity calculation as prescribed by the $\mathbf{k}\cdot\mathbf{p}$ band-structure simulation method for SWCNs within the Kubo linear-response theory [28]. To obtain the dielectric tensor of the TD array of SWCNs we use the low-energy plasmon response calculation technique proposed by one of us for finite-thickness metallic films with periodic cylindrical anisotropy [56], combined with the many-particle Green's function formalism in the Matsubara formulation [80]. With the single-tube conductivity in hand, we evaluate the collective polarization and obtain the EM response tensor for the periodic TD array of SWCNs. We also study the inhomogeneity effects for TD films composed of SWCN arrays with varied structural parameters, using the Maxwell-Garnett (MG) method [81] to obtain the EM response for weakly inhomogeneous quasiperiodic SWCN films reported experimentally [51,52].

The paper is organized as follows. Section II presents the model and formulates the Hamiltonian for the collective quasiparticle excitations in the TD plane-parallel periodic SWCN array. Section III uses this Hamiltonian to obtain the array collective polarization in terms of the surface conductivity of the individual constituent SWCN, followed by the in-plane EM response tensor derivation for the TD array, including the case of weakly inhomogeneous quasiperiodic SWCN films. Section IV discusses our findings and numerical results. Conclusions are drawn in Sec. V. Mathematical details are collected in the two appendices. We use the Gaussian units throughout unless otherwise stated.

II. THE MODEL OF COLLECTIVE EXCITATIONS

The model system we consider is presented in Fig. 1. A horizontal array of parallel aligned (y direction) identical SWCNs of radius R and length L has the translational unit Δ and width $L_\perp$ (x direction). The array is embedded in a dielectric of thickness d to form a composite layer with the effective permittivity ϵ, which is sandwiched between the substrate and superstrate with the dielectric permittivities ϵ_1 and ϵ_2, respectively. The structural parameters of the array obey the set of constraints as follows $2R \le \Delta \le d \ll L \sim L_\perp$ with R and Δ being much less than the wavelength of the light radiation. The SWCN of the (m,n) type ($n \le m$) has the radius $R = (\sqrt{3}\ b/2\pi)\sqrt{m^2+mn+n^2}$, where $b = 1.42$ Å is the C-C interatomic distance, with the electron charge density constrained by cylindrical symmetry to be uniformly distributed over its surface. The positive background of nuclei keeps the entire system electrically neutral.

We consider the most interesting case of $\epsilon \gg \epsilon_1+\epsilon_2$. In this case, with d decreasing and getting less than the in-plane distance between a pair of electrons in the composite layer, due to the strong vertical confinement their Coulomb interaction is mostly contributed by the region outside of the layer, whereby the Coulomb interaction potential loses its z-coordinate dependence and turns into the Keldysh-Rytova (KR) potential [82]. This brings our system, the array, in the TD regime where the dimensionality of the system is reduced from 3D to 2D and the only remnant of the z direction is the layer thickness d to represent the size of the vertical confinement. In our case here, it is natural to take advantage of the homogeneous electron charge distribution over the SWCN cylindrical surfaces, whereby the pair electrostatic potential can be expressed in terms of that of two uniformly charged rings of radius R each [83]. For two such rings of the unit cells at points $\boldsymbol{\rho}_n$ and $\boldsymbol{\rho}_l'$ of tubules n and l as shown in Fig. 1, the electrostatic interaction potential can be written in terms of the

symmetry-adapted KR potential as follows [56]:

$$V(\boldsymbol{\rho}_n - \boldsymbol{\rho}_l') = \frac{m^*}{N_{2D} L L_\perp} {\sum_{\mathbf{k}}}' \left[\frac{\omega_p(k)}{k}\right]^2 e^{i\mathbf{k}\cdot(\boldsymbol{\rho}_n - \boldsymbol{\rho}_l')}. \quad (1)$$

Here, $\mathbf{k} = \mathbf{q} + \mathbf{k}_\perp$ is the in-plane electron quasimomentum with $\mathbf{q}$ and $\mathbf{k}_\perp$ representing its components in the y and x direction—parallel and perpendicular to the CN alignment direction, respectively; $k = |\mathbf{k}| = \sqrt{q^2 + k_\perp^2}$, where $q = 2\pi n_y/L, n_y = 0, \pm 1, \pm 2, \ldots, \pm N/2, N = L/a, a$ is the CN lattice translation period, and $k_\perp = 2\pi n_x/L_\perp$, where $n_x = 0, \pm 1, \pm 2, \ldots, \pm N_\perp/2$, $N_\perp$ is the total number of tubules in the parallel array. The summation is primed to eliminate the $\mathbf{k} = 0$ term associated with the all-together electron displacement, $\boldsymbol{\rho}_n \neq \boldsymbol{\rho}_l{}'$ for the $n = l$ case to exclude the self-interaction, and the orthogonality condition

$$\delta_{\boldsymbol{\rho}_n \boldsymbol{\rho}_l'} = \delta_{x_n x_l'} \delta_{y_n y_l'} = \frac{1}{N_\perp N} \sum_{\mathbf{k}} e^{i\mathbf{k}\cdot(\boldsymbol{\rho}_n - \boldsymbol{\rho}_l')}$$
$$= \frac{1}{N_\perp} \sum_{k_\perp = -\pi/\Delta}^{\pi/\Delta} e^{ik_\perp (x_n - x_l')} \frac{1}{N} \sum_{q=-\pi/a}^{\pi/a} e^{iq(y_n - y_l')} \quad (2)$$

is used for the Fourier expansion basis function set in the first Brillouin zone of the array, with its reciprocal given by

$$\delta_{\mathbf{k}\mathbf{k}'} = \delta_{k_\perp k_\perp'} \delta_{qq'} = \frac{1}{N_\perp N} \sum_{\boldsymbol{\rho}_n} e^{i(\mathbf{k} - \mathbf{k}')\cdot \boldsymbol{\rho}_n}$$
$$= \frac{1}{N_\perp} \sum_{x_n = -L_\perp/2}^{L_\perp/2} e^{i(k_\perp - k_\perp')x_n} \frac{1}{N} \sum_{y_n = -L/2}^{L/2} e^{i(q-q')y_n}. \quad (3)$$

The quantity

$$\omega_p(k) = \sqrt{\frac{4\pi e^2 N_{2D}}{m^* \epsilon\, d} \frac{2qRI_0(qR)K_0(qR)}{1 + (\epsilon_1 + \epsilon_2)/(k\epsilon\, d)}} \quad (4)$$

stands for the intraband plasma oscillation frequency for a general finite-thickness, cylindrically anisotropic, periodically aligned (metallic or semiconducting) array [56]. Here, m^* is the electron effective mass, $N_{2D} (= N_{3D} d)$ is the surface electron density, I_0 and K_0 are the zeroth-order modified cylindrical Bessel functions responsible for the correct normalization of the electron density distribution over cylindrical surfaces, to give for $R \to \infty$ [whereby $qRI_0(qR)K_0(qR) \to 1/2$] the isotropic TD film plasma frequency studied previously [55].

A. The Hamiltonian

For an individual SWCN, absorption of a photon by a valence-band electron excites it to the conduction band to create an exciton. This makes a longitudinal polarization effect with an induced dipole moment directed predominantly along the nanotube axis due to a strongly suppressed SWCN polarizability in the perpendicular direction [84,85], also known as the transverse depolarization [28,86]. For a densely packed periodically aligned array of SWCNs, the induced intertubule dipole-dipole coupling should then result in the anisotropic collective polarization of the array (predominantly along the CN alignment direction), leading to the anisotropic dielectric response—the focus of our study here.

The second quantized Hamiltonian of the free exciton (see, e.g., Refs. [80,87]) on the SWCN surface can be written in the form

$$\hat{H}_{ex} = \sum_{s,q} E_s(q) B_{s,q}^\dagger B_{s,q}, \quad (5)$$

where the operators $B_{s,q}^\dagger$ and $B_{s,q}$ create and annihilate, respectively, the exciton with the longitudinal quasimomentum q (y direction in Fig. 1) in the s subband, which for the (m,n)-type SWCN is associated with the quantized circumferential momentum component $\hbar s/R$, $s = 1, 2, \ldots, m\ (\geq n)$ [34,37]. These operators satisfy the standard bosonic commutation relations

$$\left[B_{s,q}, B_{s',q'}^\dagger\right] = \delta_{ss'}\delta_{qq'}, \quad \left[B_{s,q}, B_{s',q'}\right] = 0$$

and can be converted into their coordinate counterparts using Eq. (2), to obtain

$$B_{s,y_n}^\dagger = \frac{1}{\sqrt{N}} \sum_q B_{s,q}^\dagger e^{iqy_n}, \quad B_{s,y_n} = \left(B_{s,y_n}^\dagger\right)^\dagger \quad (6)$$

for the nth SWCN of the array. The exciton energy is

$$E_s(q) = E_{exc}^{(f)}(s) + \frac{\hbar^2 q^2}{2M_{ex}(s)}, \quad (7)$$

where the first term is the excitation energy of the f-internal-state exciton, given by $E_{exc}^{(f)}(s) = E_g(s) + E_b^{(f)}(s)$ with $E_b^{(f)}(s)$ being its (negative) binding energy and E_g representing the band gap, and the second term is the translational kinetic energy of the exciton with the total effective mass M_{ex} (the sum of the subband-dependent electron and hole effective masses). The exciton on the nth SWCN of the array is produced by the absorption of a photon of the external EM radiation. This initiates the interband dipole electronic transitions $\langle s,f\,|\hat{\mathbf{d}}(\boldsymbol{\rho}_n)|0\rangle$ to create the dipole polarization, an observable quantity proportional to $|\sum_{f,\boldsymbol{\rho}_n} \langle s,f\,|\hat{\mathbf{d}}(\boldsymbol{\rho}_n)|0\rangle|^2$, mainly along the CN axis. Only the ground-internal-state (longest-lived) excitons are considered in what follows and so the f index is omitted for brevity.

The total Hamiltonian of our model system in Fig. 1 can now be written as

$$\hat{H} = \hat{H}_{\rm ex} + \hat{H}_{\rm int}, \tag{8}$$

where the second term is responsible for the collective excitations of the SWCN array originally created by the external EM radiation on an individual constituent SWCN. To obtain this part, we perform the series expansion of the electron interaction potential, Eq. (1), about the equilibrium positions of the electron density distribution. Introducing $\boldsymbol{\rho}_n + \boldsymbol{\beta}_n$ for the electron ring position displaced by a vector $\boldsymbol{\beta}_n = \boldsymbol{\beta}(\boldsymbol{\rho}_n)$ from the point $\boldsymbol{\rho}_n$ of the nth SWCN electron density distribution (and same for $\boldsymbol{\rho}'_l$; see Fig. 1), the exponential factor in Eq. (1) is expanded to the third nonvanishing term assuming that $|\boldsymbol{\rho}_n - \boldsymbol{\rho}'_l| > |\boldsymbol{\beta}_n - \boldsymbol{\beta}'_l|$, to give

$$e^{i\mathbf{k}\cdot\boldsymbol{\rho}_{nl}}\big[1 + i\mathbf{k}\cdot\boldsymbol{\beta}_{nl} - \frac{1}{2}\big(\mathbf{k}\cdot\boldsymbol{\beta}_{nl}\big)^2\big].$$

Here, $\boldsymbol{\rho}_{nl} = \boldsymbol{\rho}_n - \boldsymbol{\rho}'_l$ and $\boldsymbol{\beta}_{nl} = \boldsymbol{\beta}_n - \boldsymbol{\beta}'_l$ with the primes still to indicate that the self-interaction in the $n = l$ case is to be excluded. For achiral $(m, 0)$ and (m, m) type SWCNs (zigzag and armchair type, respectively) we choose to focus on here, the second term in square brackets vanishes due to the presence of the inversion symmetry. This is generally not true for chiral SWCNs, where it is nonzero and turns out to be the most relevant one. This case will be addressed elsewhere separately.

The extra electron potential energy that comes out of Eq. (1) due to the relative electron ring displacement $\boldsymbol{\beta}_{nl}$, is given by $\sum_{\boldsymbol{\rho}_n,\boldsymbol{\rho}'_l}\big[V(\boldsymbol{\rho}_{nl} + \boldsymbol{\beta}_{nl}) - V(\boldsymbol{\rho}_{nl})\big]$, where the summation runs over all tubules of the array and over their individual unit cells with the self-interaction excluded. With the series expansion above and the self-interaction terms dropped, this becomes

$$\frac{m^*}{N_{2\rm D}LL_\perp}\sum_{\mathbf{k},\boldsymbol{\rho}_n,\boldsymbol{\rho}'_l} e^{i\mathbf{k}\cdot\boldsymbol{\rho}_{nl}}\Big[\frac{\omega_p(k)}{k}\Big]^2\big(\mathbf{k}\cdot\boldsymbol{\beta}_n\big)\big(\mathbf{k}\cdot\boldsymbol{\beta}'_l\big),$$

and can further be rewritten as follows:

$$\frac{1}{v_0}\sum_{\mathbf{k},\boldsymbol{\rho}_n,\boldsymbol{\rho}'_l,\mu,\nu} e^{i\mathbf{k}\cdot\boldsymbol{\rho}_n}\sqrt{\frac{m^*d}{N_{2\rm D}N_\perp N}}\,\omega_p(k)\Big[\beta_{n\mu}T_{\mu\nu}(\mathbf{k})\beta'_{l\nu} + \frac{1}{2}\,\beta_{n\mu}\beta'_{l\nu}\delta_{\mu\nu}\Big]\sqrt{\frac{m^*d}{N_{2\rm D}N_\perp N}}\,\omega_p(k)\,e^{-i\mathbf{k}\cdot\boldsymbol{\rho}'_l}. \tag{9}$$

Here, $v_0 = a\Delta d$ is the elementary cell volume of the array and the second-rank tensor

$$T_{\mu\nu}(\mathbf{k}) = \frac{k_\mu k_\nu}{k^2} - \frac{\delta_{\mu\nu}}{2}\,, \quad \mu,\nu = x,y \tag{10}$$

represents the Fourier transform of the pair dipole-dipole interaction between the SWCNs in the array [80]. The second term in the square brackets equals zero. This can be proven by first summing it up over $\boldsymbol{\rho}'_l$ using Eq. (3), followed by summation over $\mathbf{k}$, which leads to $\omega_p^2(0) = 0$.

The dipole-dipole interaction energy in Eq. (9) can be used to obtain the $\hat{H}_{\rm int}$ part of the total Hamiltonian (8). Consider the real vector quantity

$$\mathbf{d}(\boldsymbol{\rho}_n) = \sqrt{\frac{m^*d}{4\pi N_{2\rm D}}}\,\omega_p(k)\boldsymbol{\beta}(\boldsymbol{\rho}_n) = \sqrt{\frac{m^*d}{4\pi N_{2\rm D}N}}\,\omega_p(k)\beta\mathbf{e}(\boldsymbol{\rho}_n), \tag{11}$$

with the unit vector $\mathbf{e}(\boldsymbol{\rho}_n) = \boldsymbol{\beta}(\boldsymbol{\rho}_n)/\beta(\boldsymbol{\rho}_n)$ to define the direction of the electron ring displacement $\boldsymbol{\beta}(\boldsymbol{\rho}_n)$ and

$$\beta = \sqrt{|\sum_{\boldsymbol{\rho}_n}\boldsymbol{\beta}(\boldsymbol{\rho}_n)|^2} \approx \sqrt{\sum_{\boldsymbol{\rho}_n}|\boldsymbol{\beta}(\boldsymbol{\rho}_n)|^2} = \sqrt{N}\beta(\boldsymbol{\rho}_n)$$

to represent the net electron density displacement (consistent with the random phase approximation and equivalency of rings) for the entire nth SWCN. Let Eq. (11) be a matrix element $\langle s,\boldsymbol{\rho}_n|\hat{\mathbf{d}}(\boldsymbol{\rho}_n)|0\rangle$ of the (Hermitian) induced dipole-moment operator defined in the second quantization form as

$$\hat{\mathbf{d}}(\boldsymbol{\rho}_n) = \sqrt{\frac{m^*d}{4\pi N_{2\rm D}N}}\,\omega_p(k)\sum_s\langle s|\hat{\boldsymbol{\beta}}|0\rangle\big(B_{s,\boldsymbol{\rho}_n} + B^\dagger_{s,\boldsymbol{\rho}_n}\big), \tag{12}$$

$$\langle s|\hat{\boldsymbol{\beta}}|0\rangle^\dagger = \langle 0|\hat{\boldsymbol{\beta}}|s\rangle^* = \langle 0|\hat{\boldsymbol{\beta}}|s\rangle = \langle s|\hat{\boldsymbol{\beta}}|0\rangle,$$

where $\hat{\boldsymbol{\beta}}$ is the quantum displacement operator to represent the classical displacement $\beta\mathbf{e}(\boldsymbol{\rho}_n)$. Then the Fourier transform

$$\hat{\mathbf{d}}(\mathbf{k}) = \frac{1}{\sqrt{N_\perp N}}\sum_{\boldsymbol{\rho}_n}\hat{\mathbf{d}}(\boldsymbol{\rho}_n)e^{-i\mathbf{k}\cdot\boldsymbol{\rho}_n}, \quad \hat{\mathbf{d}}^\dagger(\mathbf{k}) = \hat{\mathbf{d}}(-\mathbf{k}),$$

obtained using Eqs. (2) and (3), takes the form

$$\hat{\mathbf{d}}(\mathbf{k}) = \sqrt{\frac{m^*d}{4\pi N_{2\rm D}N}}\,\omega_p(k)\sum_s\langle s|\hat{\boldsymbol{\beta}}|0\rangle\big(B_{s,\mathbf{k}} + B^\dagger_{s,-\mathbf{k}}\big), \tag{13}$$

$$B_{s,\mathbf{k}} = \frac{1}{\sqrt{N_\perp N}}\sum_{\boldsymbol{\rho}_n}B_{s,\boldsymbol{\rho}_n}e^{-i\mathbf{k}\cdot\boldsymbol{\rho}_n}$$

with the creation and annihilation operators of the same meaning as those in Eqs. (5), and (9) suggests that

$$\hat{H}_{\rm int} = \frac{4\pi}{v_0}\sum_{\mathbf{k},\mu,\nu}\hat{d}_\mu(\mathbf{k})T_{\mu\nu}(\mathbf{k})\hat{d}_\nu(-\mathbf{k}). \tag{14}$$

More explicitly

$$\hat{H}_{\rm int} = \frac{1}{2}\sum_{\mathbf{k},s,s'} V_{ss'}(\mathbf{k})\big(B_{s,\mathbf{k}}+B^{\dagger}_{s,-\mathbf{k}}\big)\big(B_{s',-\mathbf{k}}+B^{\dagger}_{s',\mathbf{k}}\big), \quad (15)$$

$$V_{ss'}(\mathbf{k}) = \frac{2m^*\omega_p^2(k)d}{N_{\rm 2D}N\upsilon_0}\sum_{\mu,\nu}\langle 0|\hat{\beta}_\mu|s\rangle T_{\mu\nu}(\mathbf{k})\langle s'|\hat{\beta}_\nu|0\rangle.$$

Here, different spatial component matrix elements of the displacement operator $\hat{\boldsymbol{\beta}}$ in $V_{ss'}$ are different, in general.

In the case where the (dominant) longitudinal induced SWCN polarization is only taken into consideration and the transverse one is neglected, one has $\beta_{n\mu} = \beta_{ny}\delta_{y\mu}$ and $\beta'_{l\nu} = \beta'_{ly}\delta_{y\nu}$ in Eq. (9). This, after summing up over x_n and x'_l with Eq. (3), projects it on the y direction to give

$$\frac{1}{\upsilon_0}\sum_{q,y_n,y'_l} e^{iqy_n}\sqrt{\frac{m^*d}{N_{\rm 2D}N}}\,\omega_p(q)\,\beta_{ny} \times\; T_{yy}(q)\,\beta'_{ly}\sqrt{\frac{m^*d}{N_{\rm 2D}N}}\,\omega_p(q)\,e^{-iqy'_l},$$

where $T_{yy}(q) = T_{yy}(q, k_\perp = 0) = 1/2$ according to Eq. (10) and $\omega_p(q) = \omega_p(q, k_\perp = 0)$, thus yielding

$$\hat{H}_{\rm int} = \frac{2\pi}{\upsilon_0}\sum_q \hat{d}_y(q)\hat{d}_y(-q) = \frac{2\pi}{\upsilon_0}\sum_q \hat{d}_y(q)\hat{d}_y^{\,\dagger}(q),$$

$$\hat{d}_y(q) = \sqrt{\frac{m^*d}{4\pi N_{\rm 2D}N}}\,\omega_p(q)\sum_s \langle s|\hat{\beta}_y|0\rangle\big(B_{s,q}+B^{\dagger}_{s,-q}\big) \quad (16)$$

for Eq. (14) and

$$\hat{H}_{\rm int} = \frac{1}{2}\sum_{s,q} V_{ss}(q)\big(B_{s,q}+B^{\dagger}_{s,-q}\big)\big(B_{s,-q}+B^{\dagger}_{s,q}\big), \quad (17)$$

$$V_{ss}(q) = \frac{m^*\omega_p^2(q)d}{N_{\rm 2D}N\upsilon_0}\,|\langle s|\hat{\beta}_y|0\rangle|^2$$

for Eq. (15), respectively. In this latter case, $V_{ss'}$ takes the diagonal form $V_{ss}\delta_{ss'}$ to include only the collinear-anticollinear dipole-moment coupling between the nanotubes of the array. This is the case of practical relevance we focus on in what follows.

B. The dispersion of collective excitations

With the interaction term of Eq. (17), the total Hamiltonian (8) of the SWCN array is of the form

$$\hat{H} = \sum_{s,q}\Big[E_s(q)B^{\dagger}_{s,q}B_{s,q} + \frac{1}{2}\,V_{ss}(q)\big(B_{s,q}+B^{\dagger}_{s,-q}\big)\big(B_{s,-q}+B^{\dagger}_{s,q}\big)\Big], \quad (18)$$

which can be diagonalized exactly by means of the canonical transformation technique [88]. More specifically, the Hamiltonian such as this can be brought to the form

$$\hat{H} = \sum_{s,q}\hbar\omega_s(q)\xi^{\dagger}_s(q)\xi_s(q) + E_0 \quad (19)$$

by redefining the original exciton operators as follows:

$$B_{s,q} = u_s(q)\,\xi_s(q) + v_s(q)\,\xi^{\dagger}_s(-q), \quad (20)$$

$$|u_s(q)|^2 - |v_s(q)|^2 = 1, \quad (21)$$

in terms of the linear superposition of the collective boson excitation operators $\xi_s(q)$ representing the *eigen* states of the entire system, the array. The reciprocal of this is

$$\xi_s(q) = u^*_s(q)B_{s,q} - v_s(q)B^{\dagger}_{s,-q} \quad (22)$$

$$\big[\xi_s(q), \xi^{\dagger}_{s'}(q')\big] = \delta_{ss'}\delta_{qq'}. \quad (23)$$

The unknown transformation coefficients $u_s(q)$ and $v_s(q)$, and the eigen-state energies $\hbar\omega_s(q)$ can be found from the operator identity

$$\hbar\omega_s(q)\xi_s(q) = \big[\xi_s(q),\,\hat{H}\big], \quad (24)$$

followed by finding the vacuum (no excitations present) energy E_0 from the comparison of Eqs. (18) and (19) after the eigen-state energies and the transformation coefficients have been obtained.

Putting Eqs. (22) and (18) into Eq. (24) and equating the coefficients in front of the exciton creation and annihilation operators on the left and right side, one obtains the set of two simultaneous algebraic equations as follows:

$$\big[\hbar\omega_s(q) - E_s(q) - V_{ss}(q)\big]u_s(q) - V_{ss}(q)v_s(q) = 0,$$
$$V_{ss}(q)u_s(q) + \big[\hbar\omega_s(q) + E_s(q) + V_{ss}(q)\big]v_s(q) = 0. \quad (25)$$

Being supplemented by the extra constraint, Eq. (21), these simultaneous equations define the transformation coefficients $u_s(q)$ and $v_s(q)$ uniquely. The condition of the nontrivial solution existence requires that the determinant of Eq. (25) be equal to zero. This gives the collective excitation eigen energies in the form

$$\hbar\omega_s(q) = \sqrt{E_s^2(q) + 2E_s(q)V_{ss}(q)}, \quad (26)$$

with $E_s(q)$ given by Eq. (7), $V_{ss}(q)$ defined in Eq. (17), and $s = 1, 2, \ldots, m$ ($\geq n$) representing the excitation subbands for the periodic array composed of the (m, n) type SWCNs.

Using Eq. (26), the transformation coefficients come out of Eq. (25) in the compact form as follows:

$$u_s(q) = \frac{E_s(q) + \hbar\omega_s(q)}{2\sqrt{E_s(q)\hbar\omega_s(q)}},\ v_s(q) = \frac{E_s(q) - \hbar\omega_s(q)}{2\sqrt{E_s(q)\hbar\omega_s(q)}}. \tag{27}$$

Finally, substituting Eq. (22) in Eq. (19), using Eqs. (26) and (27) for simplifications, and comparing the end result with Eq. (18), one obtains the vacuum state energy of the array in the form

$$E_0 = \frac{1}{2}\sum_{s,q}\big[\hbar\omega_s(q) - E_s(q)\big]. \tag{28}$$

Equations (19), (22), (23), and (26)–(28) solve the dispersion relation problem for the intrinsic collective excitations in the ultrathin periodic SWCN array. One can now see that the excited *eigen* states of the SWCN array involve not only the single-tube excitons of energy $E_s(q)$ as one might expect naturally, but also the array collective plasma oscillations of energy $\hbar\omega_p(q)$ given by Eq. (4) are involved, which in the TD regime can be effectively controlled by varying the array thickness [56].

III. THE ARRAY DIELECTRIC RESPONSE

Knowing the dispersion of the excited collective quasiparticle *eigen* states of the planar SWCN array, allows one to calculate its in-plane dielectric response tensor. A relatively easy way to do this is to use the complex-frequency finite-temperature Matsubara Green's function formalism (see, e.g., Refs. [80,89]). All measurable collective quantities, such as conductivities and susceptibilities, are represented by correlation functions expressed for causality in terms of the retarded Green's functions, which can be obtained from their equivalent complex-frequency Matsubara counterparts with $i\omega = 2n\pi/\hbar\beta$ for bosons and $i\omega = (2n+1)\pi/\hbar\beta$ for fermions (n is an integer and $\beta = 1/k_BT$) by simply changing $i\omega$ to $\omega + i\delta$ with δ representing an infinitesimal energy relaxation rate [80].

A. The collective polarization

We proceed with the polarizability tensor calculation for the SWCN array within the Matsubara formalism. This is given by the correlator of the SWCN induced dipole-moment operator in Eq. (16) with itself, and this includes only one CN-related component, $P_{yy}(q, i\omega)$, since the minor polarization perpendicular to the CN axis is agreed to be neglected. Specifically,

$$P_{yy}(q, i\omega) = -\frac{1}{\hbar}\int_0^{\hbar\beta} d\tau\ e^{i\omega\tau}\langle T_\tau \hat{d}_y(q,\tau)\hat{d}_y(-q,0)\rangle, \tag{29}$$

where the bracket $\langle\ldots\rangle$ notates the thermodynamical averaging, τ $(=it)$ is the complex time, and T_τ is the ordering operator to place the (Heisenberg picture) dipole-moment operators with the earliest τ to the right.

A straightforward way to calculate Eq. (29) is by using Eq. (20) to write the single-tube induced dipole operators in terms of their collective excitation counterparts, followed by the thermodynamical averaging with the total Hamiltonian, Eq. (19), in the collective excitation Hilbert space. However, for practical use purposes it is instructive to find the connection between the single-tube excitations and the collective excitations of the entire SWCN array. To this end, we first do the averaging in Eq. (29) with the unperturbed Hamiltonian, Eq. (5), to obtain the *noninteracting* SWCN array polarizability (see Appendix A)

$$P^{(0)}_{yy}(q, i\omega) = \frac{m^*\omega_p^2(q)d}{4\pi N_{2D}N}\sum_s \frac{2E_s|\langle s|\hat{\beta}_y|0\rangle|^2}{(i\hbar\omega)^2 - E_s^2}. \tag{30}$$

Introducing the CN dynamical polarizability function

$$\alpha_{yy}(q, i\omega) = -\frac{e^2}{L}\sum_s \frac{2E_s|\langle s|\hat{\beta}_y|0\rangle|^2}{(i\hbar\omega)^2 - E_s^2} \tag{31}$$

links Eq. (30) to the optical response of an isolated CN (longitudinal polarizability per unit length) to give

$$P^{(0)}_{yy}(q, i\omega) = -\frac{m^*\omega_p^2(q)v_0}{4\pi e^2 N_{2D}\Delta}\,\alpha_{yy}(q, i\omega). \tag{32}$$

Alternatively, this can be expressed in an equivalent form in terms of the isolated CN longitudinal conductivity [28]

$$\sigma_{yy}(q, i\omega) = \frac{\hbar e^2}{2\pi RL}\sum_s \frac{-2\hbar\omega|\langle s|\hat{v}_y|0\rangle|^2}{E_s\big[(i\hbar\omega)^2 - E_s^2\big]}. \tag{33}$$

Using the relations between the velocity and coordinate displacement matrix elements

$$\langle s|\hat{v}_y|0\rangle = \langle s|\frac{d\hat{\beta}_y}{d\tau}|0\rangle = -\frac{1}{\hbar}\langle s|[\hat{\beta}_y, \hat{H}_{ex}]|0\rangle = \frac{E_s}{\hbar}\,\langle s|\hat{\beta}_y|0\rangle \tag{34}$$

and the fact that [78,79]

$$\alpha_{yy}(q, i\omega) = \frac{2\pi R}{\omega}\,\sigma_{yy}(q, i\omega), \tag{35}$$

one then obtains

$$P^{(0)}_{yy}(q, i\omega) = -\frac{m^*\omega_p^2(q)v_0}{4\pi e^2 N_{2D}\Delta}\frac{2\pi R}{\omega}\,\sigma_{yy}(q, i\omega). \tag{36}$$

Next, being performed with the total Hamiltonian, Eq. (8), the thermodynamical averaging in Eq. (29) gives the collective polarizability of the dipole-dipole *coupled* SWCN

array. This can be evaluated by a diagrammatic expansion in which the first term, given by Eq. (5), is treated as unperturbed and the second, given by Eqs. (14)–(17), is the perturbation. For the former, the noninteracting SWCN array polarizability is already known and given by Eqs. (32) and (36). A useful feature of the latter is its separability, as can be seen from Eqs. (14) and (16), so that the perturbation factors into components summed up individually. The self-energy term for the perturbation occurs in the first order with the self-energy merely equal to $2\pi/v_0$, as per Eq. (16). The higher-order terms of the diagrammatic expansion just produce multiples of this term. The overall result takes the form of the Dyson equation as follows (see Appendix B):

$$P_{yy}(q,i\omega) = P^{(0)}_{yy}(q,i\omega) + \frac{2\pi}{v_0} P^{(0)}_{yy}(q,i\omega) P_{yy}(q,i\omega),$$

which can be easily solved to give

$$P_{yy}(q,i\omega) = \frac{P^{(0)}_{yy}(q,i\omega)}{1 - 2\pi P^{(0)}_{yy}(q,i\omega)/v_0}. \tag{37}$$

This is the collective array polarization associated with the *interband* electronic transitions to create excitons on individual SWCNs embedded in a finite-thickness dielectric layer. There is also the low-energy polarization part contributed by the *intraband* transitions of harmonically bound charges on the CN surface [39,56]. The total collective polarization of the CN array is to include both intra- and interband term on an equal footing since both of them are associated with an induced oscillating dipole moment—in the lower- and higher-frequency spectral range, respectively—initially created by external EM radiation on an individual CN and spread out over the array thereafter. This can be formally done by redefining

$$\sigma_{yy}(q,i\omega) \longrightarrow \sigma^{\text{intra}}_{yy}(q,i\omega) + \sigma^{\text{inter}}_{yy}(q,i\omega) \tag{38}$$

in Eq. (36), where

$$\sigma^{\text{intra}}_{yy}(q,i\omega) = \frac{e^2 N_{2D}}{m^*} \frac{\omega}{\omega^2 + (v_F q)^2} \tag{39}$$

generally represents the single-tube intraband conductivity term with v_F being the Fermi velocity [90], and $\sigma^{\text{inter}}_{yy}$ is the interband term still given by Eq. (33). The SWCN polarizability in Eq. (32) has to be redefined per Eqs. (35) and (38) as well.

B. The dielectric response

Using Eq. (37) with $P^{(0)}_{yy}$ of Eq. (36) in the general EM response expression (Gaussian units)

$$\frac{\varepsilon_{yy}(q,i\omega)}{\epsilon} = 1 + \frac{4\pi}{v_0} P_{yy}(q,i\omega), \tag{40}$$

after simplifications one obtains the SWCN array dynamical dielectric response in the form

$$\frac{\varepsilon_{yy}(q,i\omega)}{\epsilon} = 1 - \frac{2 f_{\text{CN}}\, \sigma_{yy}(q,i\omega)}{f_{\text{CN}}\, \sigma_{yy}(q,i\omega) + \omega e^2 N_{2D} R/m^* \omega_p^2(q) d},$$

where $f_{\text{CN}} = N_\perp V_{\text{CN}}/V = \pi R^2/\Delta d$ is the CN volumetric fraction in the planar dielectric film as sketched in Fig. 1. The analytic continuation into the real frequency domain of our interest here can now be obtained by changing $i\omega$ to $\omega + i\delta$ in the above, to finally result in

$$\frac{\varepsilon_{yy}(q,\omega)}{\epsilon} = 1 - \frac{2 f_{\text{CN}}\, \sigma_{yy}(q,\omega)}{f_{\text{CN}}\, \sigma_{yy}(q,\omega) + i\omega e^2 N_{2D} R/m^* \omega_p^2(q) d} \tag{41}$$

with the longitudinal conductivity of an isolated SWCN to include both intra- and interband contributions, taking per Eqs. (38), (39), and (33) the form

$$\sigma_{yy}(q,\omega) = \sigma^{\text{intra}}_{yy} + \sigma^{\text{inter}}_{yy} = i\frac{e^2 N_{2D}}{m^*} \frac{\omega + i\delta}{(\omega + i\delta)^2 - (v_F q)^2} + \frac{\hbar e^2}{2\pi RL} \sum_s \frac{-2i\hbar\omega |\langle s|\hat{v}_y|0\rangle|^2}{E_s\left[E_s^2 - (\hbar\omega)^2 - 2i\hbar^2\omega\delta\right]}. \tag{42}$$

Here, δ takes the meaning of a (phenomenological) inverse energy relaxation time, $\delta = 1/\tau_r$, associated with the inelastic (phonon, defect) scattering [30,91] and can generally be different for intra- and interband processes.

Under continuous low-intensity light illumination, the dielectric film with the SWCN array embedded in it can still be treated as being at the thermal equilibrium. At not too low temperatures the distribution of the s-subband quasiparticle excitations over the q-momentum space is then given by the normalized Boltzmann distribution function

$$f_s(q,T) = \frac{1}{Q_s} e^{-\beta\hbar\omega_s(q)}, \tag{43}$$

with $\hbar\omega_s(q)$ representing the energy of the excited quasiparticle *eigen* states of the SWCN array given by Eq. (26) and the normalization factor is

$$Q_s = \sum_q e^{-\beta\hbar\omega_s(q)} = \frac{L}{\pi\hbar}\sqrt{\frac{M_s}{2}} \int_{E_{\text{exc}}}^{\infty} \frac{dE\, e^{-\beta\hbar\omega_s(q)}}{\sqrt{E - E_{\text{exc}}(s)}},$$

with $q = \sqrt{2M_s\,[E - E_{\text{exc}}(s)]}/\hbar$ to be used in the integral. The thermal averaging of Eq. (41) with this distribution

function gives the temperature dependence of the EM response of the SWCN array in the form

$$\varepsilon_{yy}(T,\omega) = \sum_q f_s(q,T)\,\varepsilon_{yy}(q,\omega) = \frac{L}{\pi\hbar}\sqrt{\frac{M_s}{2}}\int_{E_{\rm exc}}^{\infty}\frac{dE\,f_s(q,T)\,\varepsilon_{yy}(q,\omega)}{\sqrt{E-E_{\rm exc}(s)}}. \quad (44)$$

Equations (41)–(44) and (26) provide the complete description of the spatially anisotropic linear EM response of the periodically aligned SWCN array in the TD regime. This is generally a two-component spatially dispersive (nonlocal) tensor of the form

$$\hat{\varepsilon}(q,\omega) = \begin{bmatrix} \varepsilon_{xx} & 0 \\ 0 & \varepsilon_{yy} \end{bmatrix} = \begin{bmatrix} \epsilon & 0 \\ 0 & \varepsilon_{yy}(q,\omega) \end{bmatrix}, \quad (45)$$

which should be averaged per Eq. (44) to represent the thickness-dependent anisotropic dynamical response to continuous low-intensity light illumination. In practice, the CN-array-embedding dielectric layer may still have inclusions of nonidentical parallel aligned CNs. Assuming their (quasi)periodic in-plane distribution, these inhomogeneities in an otherwise homogeneous SWCN array can be accounted for by means of the MG mixing method [81], whereby under continuous illumination the yy component of Eq. (45) takes the form

$$\langle\varepsilon_{yy}(T,\omega)\rangle = \sum_{\alpha=1}^{n} w_\alpha \varepsilon_{yy}^{(\alpha)}(T,\omega). \quad (46)$$

Here, $\varepsilon_{yy}^{(\alpha)}(T,\omega)$ refers to a thermally averaged homogeneous component of weight

$$w_\alpha = \frac{f_{\rm CN}^{(\alpha)}}{\sum_{i=1}^{n} f_{\rm CN}^{(i)}} = \left[\sum_{i=1}^{n}\left(\frac{R_i}{R_\alpha}\right)^2\frac{\Delta_\alpha}{\Delta_i}\right]^{-1} \quad (47)$$

in the generally n-component inhomogeneous mixture of periodic (or quasiperiodic) SWCN arrays with radii R_α and intertube separation distances Δ_α, which is embedded in the finite-thickness dielectric layer. The weights are defined to give $\sum_{\alpha=1}^{n} w_\alpha = 1$, accordingly.

IV. DISCUSSION

One can see from Eq. (26) that the intertube dipole-dipole interaction, Eq. (17), makes the CN array collective spatial dispersion $\hbar\omega_s(q)$ greatly different from the isolated-CN spatial dispersion $E_s(q)$ in Eq. (7) due to the nonzero ratio $V_{ss}(q)/E_s(q)$. This is a q-dependent function inversely proportional to $\Delta \in (2R,+\infty)$, which only tends to zero to give $\hbar\omega_s(q) = E_s(q)$ in the limit of $\Delta \to +\infty$. For small momenta q controlling the most of the q-space quasiparticle state population, the major q dependence comes from the linear dependence of $\omega_p^2(q) \sim q$ in $V_{ss}(q)$ [see Eq. (4)] rather than from the quadratic dependence of $E_s(q) \sim q^2$, which is why [as well as in view of the fact that $\hbar^2q^2/2M_{\rm ex} \ll E_{\rm exc}$ in Eq. (7)] the second-order q^2 dispersion can be ignored for the qualitative analysis. With this in mind, comparing Eqs. (17) and (42) with Eq. (34) taken into account, one obtains an estimate

$$V_{ss}(q) \approx \frac{m^*\hbar^2\omega_p^2(q)}{e^2N_{\rm 2D}\tau_r E_s}\frac{2\pi R}{\Delta}\,\sigma_{yy}^{\rm inter}(E_s), \quad (48)$$

where $E_s = E_{\rm exc}$ and $\sigma_{yy}^{\rm inter}(E_s)$ is the $\sigma_{yy}^{\rm inter}(0,\omega = E_s/\hbar)$ single-subband approximation given by the greatest resonance term of the sum in Eq. (42). Substituting $\omega_p(q)$ of Eq. (4) in Eq. (48), one gets the ratio

$$\frac{V_{ss}(q)}{E_s} \approx g(E_s,\tau_r)\frac{2(qR)^2I_0(qR)K_0(qR)}{\epsilon qd+\epsilon_1+\epsilon_2}\frac{2\pi R}{\Delta}, \quad (49)$$

with $g(E_s,\tau_r) = 4\pi\hbar^2\sigma_{yy}^{\rm inter}(E_s)/\tau_r E_s^2 R$ being a constant.

Plugging Eq. (49) in Eq. (26) gives the graph in Fig. 2 to show the general behavior of $\hbar\omega_s(q)/E_s$ as a function of qd and $\Delta/2R$ for $R/d = 0.5$ and 0.25, the two cases where the array is enclosed in and buried inside of the dielectric layer, respectively. We use $E_s = E_{\rm exc} \approx 1$ eV and $\sigma_{yy}^{\rm inter}(E_s) \approx 100\ (e^2/2\pi\hbar)$ typical of the first-subband exciton in semiconducting SWCNs of $R \approx 1$ nm [28,36], with $\tau_r = 100$ fs typical of exciton-phonon scattering [91], to obtain $g(E_s,\tau_r) \approx 2$. The dielectric constants are set to $\epsilon = 10$ and $\epsilon_{1,2} = 1$. One can see a rapidly increasing spatial dispersion as the intertube distance shrinks. As expected, the thinner the dielectric layer ($d = 2R$ compared to $d = 4R$), the stronger the dispersion due to the dielectric screening effect reduction.

To better understand the dielectric response behavior as a function of the intrinsic parameters of the SWCN array, we rewrite Eq. (41) as follows:

$$\frac{\varepsilon_{yy}(q,\omega)}{\epsilon} = 1 - \frac{2[1+\lambda(\omega)]}{1+\lambda(\omega)+\omega(\omega+i\delta)\Delta/\omega_p^2(q)\pi R}. \quad (50)$$

Here, the array parameters are grouped in the denominator second term, the ratio

$$\lambda(\omega) = \frac{\sigma_{yy}^{\rm inter}(\omega)}{\sigma_{yy}^{\rm intra}(\omega)} \approx \sum_s \frac{\sigma_{yy}^{\rm inter}(E_s)}{\sigma_{yy}^{\rm intra}(0)}\frac{2\hbar\omega(\hbar\omega+i\hbar\delta)}{(\hbar\omega)^2-E_s^2+2i\hbar^2\omega\delta}, \quad (51)$$

where in view of Eq. (48) one has

$$\frac{\sigma_{yy}^{\rm inter}(E_s)}{\sigma_{yy}^{\rm intra}(0)} \approx \frac{E_sV_{ss}(q)}{\hbar^2\omega_p^2(q)}\frac{\Delta}{2\pi R}, \quad (52)$$

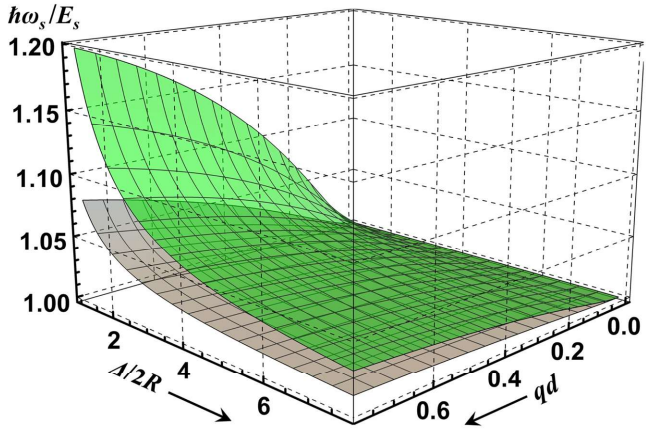

FIG. 2. Dispersion of collective excitations in the ultrathin SWCN arrays with $R/d = 0.5$ (green) and 0.25 (gray) relative to the isolated SWCN exciton dispersion as a function of array parameters qd and $\Delta/2R$.

representing the SWCN alone, and the q^2-dispersion terms are dropped. The function $\lambda(\omega)$ can be seen to rapidly diminish for $\omega \ll E_s/\hbar$, whereby in the low-frequency range $\omega_p\sqrt{\pi R/\Delta} < \omega < E_s/\hbar$ far from resonances Eq. (50) takes a spatially dispersive (nonlocal) Drude-like response form

$$\frac{\varepsilon_{yy}(q,\omega)}{\epsilon} \approx 1 - \frac{2\pi R}{\Delta}\frac{\omega_p^2(q)}{\omega(\omega+i\delta)}, \tag{53}$$

thickness, substrate, and superstrate-dependent as per Eq. (4), which (except for a geometry-specific constant prefactor) was previously reported to consistently describe the optical properties of both in-plane isotropic and cylindrically anisotropic TD plasmonic films [55–58,92].

For $\hbar\omega \sim E_s$, the function $\lambda(\omega)$ can be seen to increase dramatically, whereby Eq. (50) after straightforward simplifications using Eq. (52) takes the form

$$\frac{\varepsilon_{yy}(q,\omega)}{\epsilon} \approx 1 - \frac{2E_sV_{ss}(q)}{(\hbar\omega)^2 - \left[1 - V_{ss}(q)/E_s\right]E_s^2 + 2i\hbar^2\omega\delta},$$

which can further be compacted to give

$$\frac{\varepsilon_{yy}(q,\omega)}{\epsilon} \approx \frac{\left[(\hbar\omega)^2 - E_{s+}^2\right]\left[(\hbar\omega)^2 - E_{s-}^2\right]}{\left[(\hbar\omega)^2 - E_{s-}^2\right]^2 + \left(2\hbar^2\omega\delta\right)^2} + i\frac{4E_sV_{ss}(q)\hbar^2\omega\delta}{\left[(\hbar\omega)^2 - E_{s-}^2\right]^2 + \left(2\hbar^2\omega\delta\right)^2}, \tag{54}$$

where $E_{s\pm} = E_s\sqrt{1 \pm V_{ss}(q)/E_s}$. Here, both absorption resonance position and intensity of the EM response can be seen being adjustable by varying the array thickness, density, and dielectric parameters according to Eq. (49), whereby the ratio $V_{ss}(q)/E_s = \{[\hbar\omega_s(q)/E_s]^2 - 1\}/2$ can be adjusted that controls the difference between the collective eigen-state and single-tube exciton-state energies. The real part Re $\varepsilon_{yy}/\epsilon$ of Eq. (54) reveals the *negative refraction* (NR) band centered around E_s in the domain

$$\sqrt{E_s^2 - E_sV_{ss}(q)} = E_{s-} < \hbar\omega < E_{s+} = \sqrt{E_s^2 + E_sV_{ss}(q)} \tag{55}$$

of width $E_{s+} - E_{s-} \approx V_{ss}(q)$. The imaginary part Im $\varepsilon_{yy}/\epsilon$ of Eq. (54) and the imaginary part of its negative inverse

$$-\operatorname{Im}\frac{\epsilon}{\varepsilon_{yy}(q,\omega)} \approx \frac{4E_sV_{ss}(q)\hbar^2\omega\delta\left\{\left[(\hbar\omega)^2 - E_{s-}^2\right]^2 + \left(2\hbar^2\omega\delta\right)^2\right\}}{\left\{\left[(\hbar\omega)^2 - E_{s+}^2\right]\left[(\hbar\omega)^2 - E_{s-}^2\right]\right\}^2 + \left[4E_sV_{ss}(q)\hbar^2\omega\delta\right]^2} \tag{56}$$

are representative of the transversely polarized EM wave absorption by excitons and of the Coulomb-energy losses for longitudinally polarized plasmon excitations, respectively [93]. From Eqs. (54) and (56) E_{s-} and E_{s+} can be seen being their respective resonance peak energies. The latter is an analog of the *interband* plasmon resonance, the one situated in between the two neighboring exciton subbands [30,34]).

The range of the NR band can be found straightforwardly from the analysis of extrema for the real-valued function Re $\varepsilon_{yy}/\epsilon$ of Eq. (54). This gives

$$\left(\hbar\omega_{\min}\right)^2 \approx E_{s-}^2 + 2E_s\hbar\delta\sqrt{1 + \left[\frac{\hbar\delta}{V_{ss}(q)}\right]^2} \tag{57}$$

to the first infinitesimal order in the smallness parameter $\hbar\delta/E_s \ll 1$ and

$$\operatorname{Re}\frac{\varepsilon_{yy}(q,\omega_{\min})}{\epsilon} \approx \frac{1}{2}\left\{1 - \sqrt{1 + \left[\frac{V_{ss}(q)}{\hbar\delta}\right]^2}\right\} \tag{58}$$

to the first *nonvanishing* (zeroth) order in the same parameter. In these equations the ratio under the square root is independent of δ since $V_{ss}(q) \sim \hbar/\tau_r = \hbar\delta$ as can be seen from Eq. (49). This ratio can be controlled by means of $\Delta/2R$ to rarefy (or densify) the CN array as well as through d and $\epsilon/(\epsilon_1 + \epsilon_2)$ to adjust the array thickness and material composition, respectively. From Eqs. (55), (57), and (58) it can be seen that $\hbar\omega_{\min}$ shifts to the blue and the NR bandwidth shrinks down to zero along with its range as $V_{ss}(q)$ decreases. Clearly, originating from the intertube dipole-dipole interaction, the NR band of the homogeneous TD arrays of identical SWCNs can be controlled on demand, both to expand and to shrink, by means of adjusting these interactions as per Eq. (49).

Figure 3 shows Re $\varepsilon_{yy}/\epsilon$, Im $\varepsilon_{yy}/\epsilon$, and $-\mathrm{Im}(\epsilon/\varepsilon_{yy})$ in dimensionless variables as given by Eqs. (54), (56), and (49), to demonstrate the NR band behavior, the exciton absorption and interband plasmon response in the neighborhood of a single-tube exciton resonance as functions of the intrinsic parameters of the SWCN array. The graphs are obtained for the same material parameters as in Fig. 2. In (a) and (b), the decrease of the thickness can be seen to push the exciton and plasmon resonances closer together, quenching their intensities to reduce the NR bandwidth and range. Comparing (a) and (b), both exciton and plasmon resonance intensities can be seen being lower for the thicker dielectric layer in (b), apparently due to the greater dielectric screening effect. In (c), the overlap of the exciton and plasmon resonances can be seen to increase with the intertube distance, whereby a controllable exciton-plasmon *hybridization* is possible by varying the intrinsic parameters of the array. All these are the *universal* features of the EM response that originate from the eigen-state dispersion relations of the TD arrays of SWCNs in the domain of their interband transitions as described by Eqs. (54)–(58). Far from this domain their low-energy EM response features a thickness, substrate, and superstrate-dependent Drude-like metallic behavior given by Eq. (53).

Figures 4 and 5 present our numerical simulations to show how the thermal broadening and a slight diameter dispersion affect the EM response of a finite-thickness SWCN film in the TD regime. We start with the longitudinal (along the CN symmetry axis) dielectric functions $\varepsilon_{\parallel}(\omega)$ for the five individual zigzag SWCNs in vacuum, shown in Fig. 4(a). The SWCNs chosen are the semiconducting (16,0), (17,0), (19,0), and (20,0) CNs and the metallic (18,0) CN—all of about the same diameter centered at $2R_{(18,0)} = 1.41$ nm. Focusing on the domain around the first exciton resonance, we obtain their dielectric functions $\varepsilon_{\parallel}$ from $\sigma_{yy}^{\mathrm{inter}}$ of Eq. (42), calculated using the $\mathbf{k}\cdot\mathbf{p}$ method of the SWCN band-structure calculations [28] with $\tau_r = 100$ fs, followed by the Drude relation $\varepsilon_{\parallel}(\omega) = 1 + 8\pi i\sigma_{\parallel}(\omega)/R\omega$ [30] with $\sigma_{\parallel} = \sigma_{yy}$ of Eq. (42).

Marked in Fig. 4(a) are peaks of $\mathrm{Im}\varepsilon_{\parallel}$ and $-\mathrm{Im}(1/\varepsilon_{\parallel})$ to indicate the dipole *interband* electronic transitions E_{11} (E_{22}) and P_{11} from the CN first (second) valence band to the CN first (second) conduction band [28], to produce the first (second) exciton and the first interband plasmon, respectively. The latter one, though not that intensive, shows up in the domains where $\mathrm{Re}\varepsilon_{\parallel} = 0$ and $\mathrm{Im}\varepsilon_{\parallel} \to 0$ (or $\mathrm{Im}\sigma_{\parallel} = 0$ and $\mathrm{Re}\sigma_{\parallel} \to 0$, accordingly [30,34]) due to the Kramers-Kronig relation that links $\mathrm{Re}\varepsilon_{\parallel}$ and $\mathrm{Im}\varepsilon_{\parallel}$. The plasmon peak $P^{(18,0)}$ of the metallic (18,0) SWCN is due to the *intraband* transition that comes from $\sigma_{yy}^{\mathrm{intra}}$ of Eq. (42). As a classical plasmon resonance it is highly pronounced, while the interband (quantum) transitions occur for the (18,0) SWCN at much higher energies outside of the domain presented. For each of the nanotubes in Fig. 4(a),

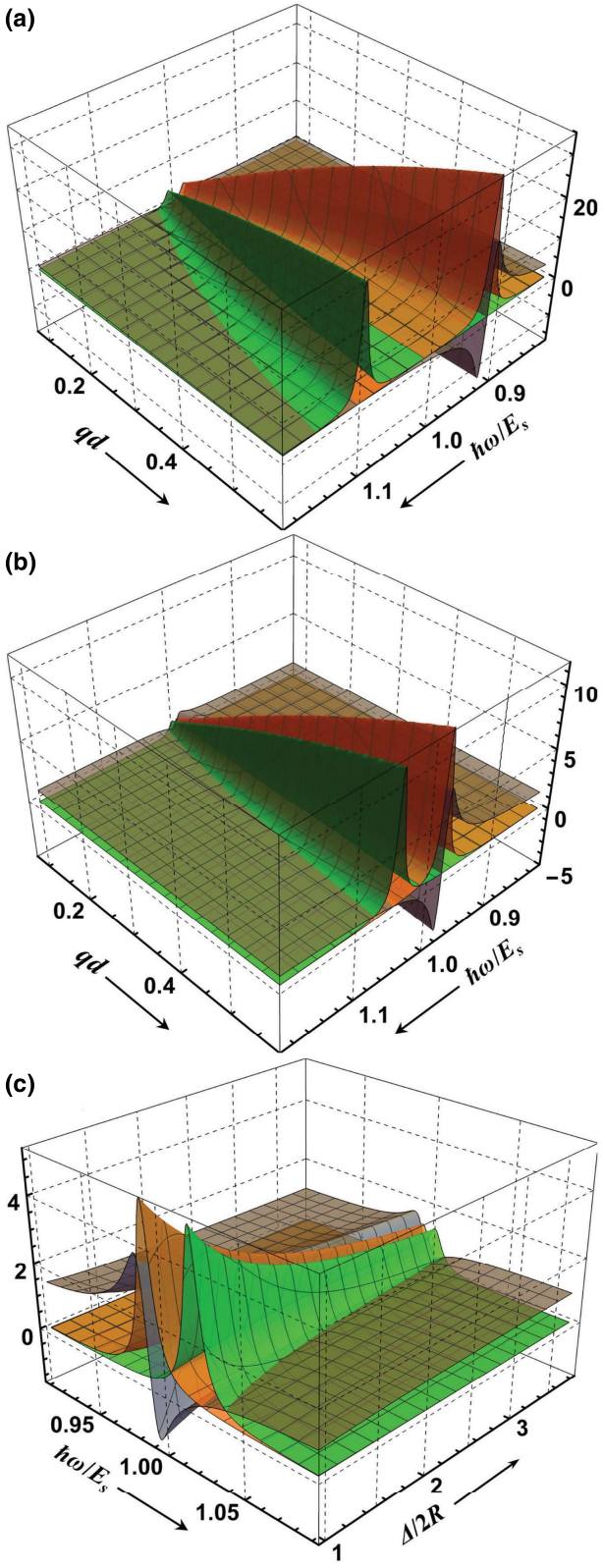

FIG. 3. Re $\varepsilon_{yy}/\epsilon$ (gray), Im $\varepsilon_{yy}/\epsilon$ (orange), and $-\mathrm{Im}(\epsilon/\varepsilon_{yy})$ (green) plotted per Eq. (54) in the exciton resonance range $\hbar\omega/E_s \sim 1$ as functions of $\hbar\omega/E_s$ and qd for dense ($\Delta/2R = 1$) ultrathin SWCN arrays with $R/d = 0.5$ (a) and 0.25 (b), and as functions of $\hbar\omega/E_s$ and $\Delta/2R$ with $R/d = 0.5$, $qd = 0.1$ (c).

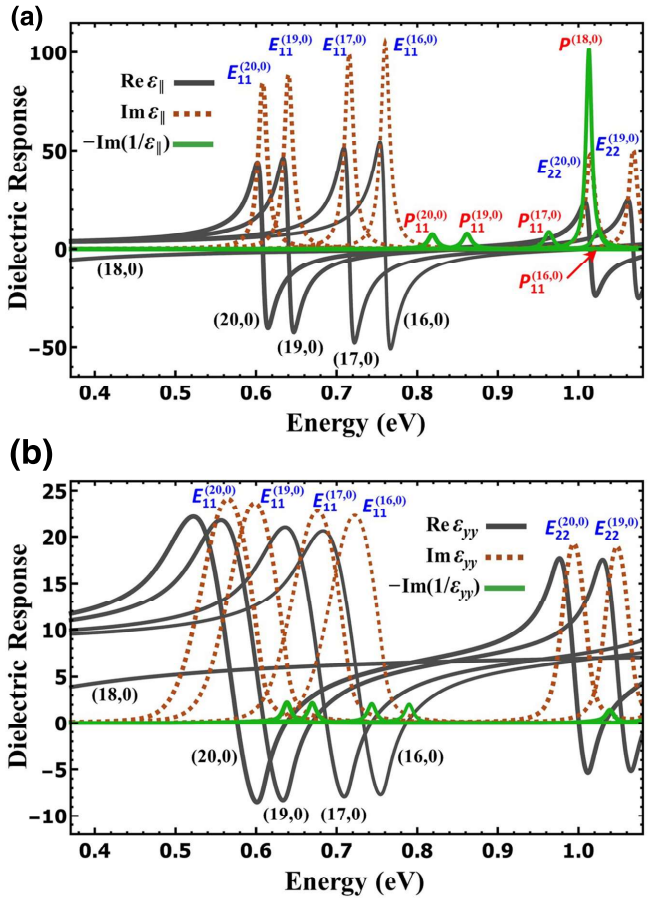

FIG. 4. (a) Individual dielectric responses along the CN axis (longitudinal) for the zigzag (16,0), (17,0), (18,0), (19,0), and (20,0) SWCNs *in vacuum*, obtained using the $\mathbf{k}\cdot\mathbf{p}$ method of the SWCN band-structure calculations [28]. All graphs are scaled down vertically by a factor of 10 for better visibility. (b) Respective room-temperature dielectric response functions along the CN alignment direction, calculated as given by Eqs. (41)–(44) for the ultrathin periodic arrays of the (16,0), (17,0), (18,0), (19,0), and (20,0) SWCNs. See text for details.

their respective dielectric response functions exhibit sharp resonance structures typical of vacuum and known to get quenched by a dielectric background [31]. To obtain the dielectric responses for the respective homogeneous SWCN arrays, presented in Fig. 4(b) in the same energy domain for comparison, we use our derived Eqs. (41)–(44) with $d = \Delta = 2R$ yielding $f_{\mathrm{CN}} = \pi/4$ for their respective R, and $T = 300$ K for each of the arrays. Other array parameters are taken to be the same for all five of them: $\epsilon = 10$, $\epsilon_1 = \epsilon_2 = 1$, the first exciton translational effective mass $M_1 = 0.4\, m_0$ (m_0 is the free electron rest mass) and the relaxation time $\tau_r = 100$ fs [30,91]. The intensity decrease and large broadening can be seen along with the red shifts of the exciton and plasmon resonances, overall just in the way prescribed universally by the single-resonance approximation as per Eqs. (54)–(58), including the presence of the NR band.

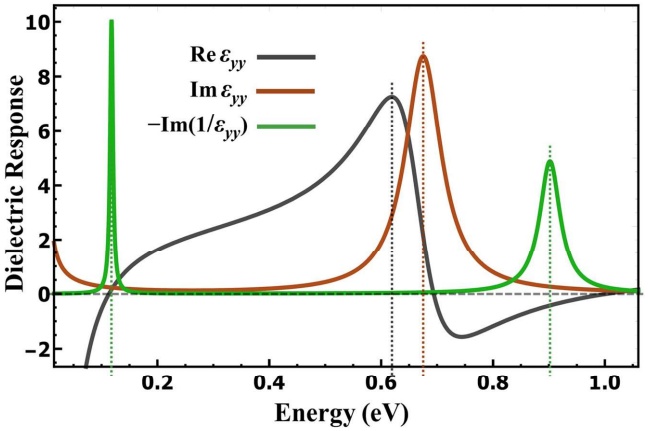

FIG. 5. The room-temperature (300 K) in-plane dielectric response functions along the CN alignment direction calculated for an ultrathin (approximately 10 nm) weakly inhomogeneous TD film of the MG-mixed (16,0), (17,0), (18,0), (19,0), and (20,0) SWCN arrays whose individual responses are presented in Fig. 4(b). See text for details.

Figure 5 presents an example of the in-plane dielectric responses along the CN alignment direction for a weakly inhomogeneous TD film made out of a quasiperiodic mixture of the (16,0), (17,0), (18,0), (19,0), and (20,0) homogeneous SWCN arrays. To obtain these graphs, we use the MG method as prescribed in Eqs. (46) and (47). For each array component in the mixture the thickness is taken to be $d = 3R$ and the intertube distances Δ_α ($\alpha = 1, ..., 5$) are set to $\Delta_{(16,0)} = 6R$, $\Delta_{(17,0)} = 2R$, $\Delta_{(18,0)} = 2R$, $\Delta_{(19,0)} = 5R$, and $\Delta_{(20,0)} = 6R$ with R being the radius of the constituent SWCN of the respective homogeneous array. The resulting weakly inhomogeneous TD film comes out to consist of the (16,0), (17,0), (18,0), (19,0), and (20,0) homogeneous SWCN arrays with the relative weights of 0.1, 0.31, 0.33, 0.14, and 0.12, respectively, to give the sum of weights equal to unity as required and to make the film be composed of about $1/3$ metallic and $2/3$ semiconducting SWCNs, which is normally the case experimentally [51,52,54]. The dielectric responses of the individual array components are calculated beforehand as described for Fig. 4(b) above. The overall thickness of this film is estimated to be approximately 10 nm. We also take into account that in a real sample there may be other CNs of different chiralities but of about the same diameter, some of them may be bent, tilted and so may not be equally spaced or precisely periodic. Therefore, the curves in Fig. 5 are smoothed out to a regular shape.

Comparing Figs. 5 and 4(b), one can see a much stronger broadening for both exciton and interband plasmon resonances of the (just weakly) inhomogeneous film. In contrast to its homogeneous SWCN array constituents,

the broaden interband plasmon resonance of the MG-mixed film is almost as intensive as the exciton resonance. Both resonances can now be seen to overlap a great deal, thus making possible the exciton-plasmon coupling and the respective exciton-plasmon hybridization. We believe this sheds more light on the nature of the ultrastrong exciton-plasmon coupling effect recently reported for self-assembled crystallized CN films experimentally [48]. The NR band of the weakly inhomogeneous TD film in Fig. 5 can be seen to expand and its range to shrink accordingly, breaking the limits set up for homogeneous periodic SWCN arrays by Eqs. (55) and (58). The classical intraband plasmon resonance, a low-energy feature of the metallic (18,0) array component described by Eq. (53) and not shown in Fig. 4(b), is presented in Fig. 5 as well. Since we have only a single metallic CN component in our model MG mixture here, this resonance comes out very narrow in the graphs presented. However, for instance, having the metallic (16,1) and (19,1) SWCNs included, with diameters of just 8 % less and greater than that of the (18,0) SWCN, respectively, would broaden this resonance inhomogeneously as well. Furthermore, in addition to the phonon scattering, intraband plasma oscillations can be strongly quenched by the Coulomb electron scattering, a scattering process that is suppressed for interband transitions forming neutral excitons, thus to result in a much stronger homogeneous broadening of the intraband plasmon resonance. In real self-assembled CN films one therefore should expect this resonance to be largely broaden, both homogeneously and inhomogeneously.

V. CONCLUSIONS

In this paper, we study the intrinsic collective quasiparticle excitations responsible for the in-plane EM response of the ultrathin plane-parallel homogeneous periodic SWCN arrays and weakly inhomogeneous SWCN films in the TD regime. We use the low-energy plasmon response calculation technique [56] combined with the many-particle Green's function formalism in the Matsubara formulation [80] to derive the dynamical dielectric tensor of the system in the broad spectral domain of microwave to visible ($\lesssim$ 1–2 eV). This is where intrinsic excitations, excitons and plasmons, are present in individual constituent SWCNs [24,29]. We use an approach that works well as applied to molecular solids where individual molecules, represented by individual nanotubes in our case, are weakly bound together by the van der Waals interaction, and the EM response of the solid (a dense periodic array or film of aligned nanotubes in our case) comes about due to a locally induced single-molecule dipole polarization propagating through the periodic lattice of molecules to create the collective polarization of the entire molecular solid. Our theory links the dynamical dielectric response tensor of the SWCN periodic array to the complex longitudinal conductivity of the constituent SWCN, a building block the array is composed of. The SWCN conductivity can be calculated by a number of numerical and analytical methods [28,29,90], of which to demonstrate the way our theory works we use the $\mathbf{k}\cdot\mathbf{p}$ method of the SWCN band-structure calculations based on the Kubo linear-response theory [28]. Our model and the results we present encompass the periodic arrays and films formed by achiral SWCNs. Arrays of chiral SWCNs require an extra analysis for collective gyrotropic effects, which we will present separately elsewhere.

We show that the collective dielectric response can be controlled by the volume fraction of constituent SWCNs, the active component of the ultrathin TD film, and that this can be done not only by varying the parameters of the SWCN content, such as the CN diameter and intertube distance, but also by merely varying the thickness of the CN embedding dielectric layer. For homogeneous single-type SWCN periodic arrays, the real part of the dielectric response function is negative for a sufficiently wide domain in the neighborhood of a quantum interband transition of the constituent SWCN, to form a relatively broad NR band that makes the system behave as a hyperbolic metamaterial at much higher frequencies than those typically in the IR domain that the classical intraband plasma oscillations have to offer [94]. By decreasing the CN diameter it is quite possible to push this NR band in the visible region, while using weakly inhomogeneous multitype SWCN films can make it even broader than that of the single-type SWCN array.

The overall behavior we obtain theoretically for the real and imaginary part of the in-plane dielectric response of the weakly inhomogeneous SWCN film is very similar to that reported experimentally for self-assembled SWCN metamaterial films in Ref. [51], which is why we believe that the NR band observed there for undoped samples is most likely due to the inhomogeneous broadening as presented in Fig. 5. Electron doping would primarily affect the intraband plasmon of a metallic CN component to largely broaden and shift it to the blue, as evidenced by our Eq. (53), due to the Coulomb scattering and electron density increase, respectively, which is precisely what was observed in Ref. [51] as well. Our theory thereby indicates that the periodically aligned, homogeneous and weakly inhomogeneous ultrathin TD films of SWCNs are excellent candidates for the development of multifunctional optical hyperbolic metasurfaces, to push the NR band and the respective hyperbolic response (typically pertinent to the IR [94]) into the optical spectral region, with characteristics adjustable on demand by means of the SWCN diameter, chirality, and periodicity variation.

ACKNOWLEDGMENTS

This research is supported by the U.S. National Science Foundation under Condensed Matter Theory Program Award No. DMR-1830874 (I.V.B.)

APPENDIX A: PROOF OF EQ. (30)

Under constant illumination by low-intensity external monochromatic radiation polarized along the nanotube alignment direction, by virtue of the linear response theory in the exciton-radiation interaction and associated fluctuation-dissipation theorem [95], the averaging over all possible SWCN array quasiparticle configurations can be done in the form of a general equilibrium statistical ensemble averaging as follows:

$$\langle \cdots \rangle = e^{\beta\Omega}\,\mathrm{Tr}\big(e^{-\beta\hat{H}}\cdots\big) \;\text{ with }\; e^{-\beta\Omega} = \mathrm{Tr}\big(e^{-\beta\hat{H}}\big), \tag{A1}$$

where $\hat{H} = \hat{H}_0 + \hat{H}_{\rm int}$ is the total Hamiltonian, Eq. (18), of the system. For the reasons explained in the main text we choose not to use the diagonalized form, Eq. (19), of the total Hamiltonian here. Instead, we proceed in the standard way [80,89], working in the noninteracting exciton Hilbert space

$$\prod_{s,q}|N_{s,q}\rangle = \prod_{s,q}\frac{\big(B^{\dagger}_{s,q}\big)^{N_{s,q}}}{\sqrt{N_{s,q}!}}|0\rangle, \tag{A2}$$

with the noninteracting particle number operator defined by equations $\hat{N}_{s,q}|N_{s,q}\rangle = B^{\dagger}_{s,q}B_{s,q}|N_{s,q}\rangle = N_{s,q}|N_{s,q}\rangle$, whereby the equilibrium statistical ensemble averaging procedure, Eq. (A1), takes the following explicit form:

$$\begin{aligned}\langle \cdots \rangle &= e^{\beta\Omega}\,\mathrm{Tr}\big[e^{-\beta(\hat{H}_0+\hat{H}_{\rm int})}\cdots\big]\\ &= e^{\beta\Omega}\prod_{s,q}\sum_{N_{s,q}=0}^{\infty}\langle N_{s,q}|\,e^{-\beta(\hat{H}_0+\hat{H}_{\rm int})}\cdots|N_{s,q}\rangle.\end{aligned} \tag{A3}$$

In particular, in the absence of the intertube interaction $\hat{H}_{\rm int}$ this takes the form

$$\begin{aligned}\langle \cdots \rangle_0 &= e^{\beta\Omega_0}\,\mathrm{Tr}\big[e^{-\beta\hat{H}_0}\cdots\big]\\ &= e^{\beta\Omega_0}\prod_{s,q}\sum_{N_{s,q}=0}^{\infty}\langle N_{s,q}|\,e^{-\beta\hat{H}_0}\cdots|N_{s,q}\rangle,\end{aligned} \tag{A4}$$

with

$$\begin{aligned}e^{-\beta\Omega_0} &= \mathrm{Tr}\big(e^{-\beta\hat{H}_0}\big)\\ &= \prod_{s,q}\sum_{N_{s,q}=0}^{\infty}\langle N_{s,q}|\,e^{-\beta\sum_{s',q'}E_{s'}(q')\hat{N}_{s',q'}}|N_{s,q}\rangle\\ &= \prod_{s,q}\frac{1}{1-e^{-\beta E_s(q)}}.\end{aligned} \tag{A5}$$

This consistently gives the mean exciton occupation number of a noninteracting boson form

$$\bar{N}_{s,q} = \langle\hat{N}_{s,q}\rangle_0 = \langle B^{\dagger}_{s,q}B_{s,q}\rangle_0 = \frac{1}{e^{\beta E_s(q)}-1}, \tag{A6}$$

with no chemical potential in it since only one exciton can be thought of being present in the system at a time, which is typically the case for not too high irradiation intensity.

For the *noninteracting* SWCN array the averaging in Eq. (29) takes the form

$$\begin{aligned}\langle T_\tau\hat{d}_y(q,\tau)\hat{d}_y(-q,0)\rangle_0 &= \Theta(\tau)\langle\hat{d}_y(q,\tau)\hat{d}_y(-q,0)\rangle_0\\ &+\Theta(-\tau)\langle\hat{d}_y(-q,0)\hat{d}_y(q,\tau)\rangle_0,\end{aligned} \tag{A7}$$

where $\Theta(\tau)$ is the theta-function, to give

$$P^{(0)}_{yy}(q,i\omega) = -\frac{1}{\hbar}\int_0^{\hbar\beta}d\tau\;e^{i\omega\tau}\langle\hat{d}_y(q,\tau)\hat{d}_y(-q,0)\rangle_0, \tag{A8}$$

with

$$\hat{d}_y(q,\tau) = e^{\tau\hat{H}_0}\hat{d}_y(q)e^{-\tau\hat{H}_0} \tag{A9}$$

and the (Schrödinger picture) induced dipole-moment operator $\hat{d}_y(q)$ defined in terms of the exciton creation and annihilation operators as per Eq. (16). Using the Baker-Hausdorff lemma (see, e.g., Ref. [96])

$$\begin{aligned}e^{\hat{A}}\hat{C}e^{-\hat{A}} &= \hat{C}+[\hat{A},\hat{C}]+\frac{1}{2!}[\hat{A},[\hat{A},\hat{C}]]\\ &+\frac{1}{3!}[\hat{A},[\hat{A},[\hat{A},\hat{C}]]]+\;\ldots\end{aligned}$$

it is easy to show that

$$e^{\tau\hat{H}_0}B_{s,q}e^{-\tau\hat{H}_0} = e^{-\tau E_s}B_{s,q}, \quad e^{\tau\hat{H}_0}B^\dagger_{s,q}e^{-\tau\hat{H}_0} = e^{\tau E_s}B^\dagger_{s,q}. \tag{A10}$$

Inserting Eqs. (A9) and (A10) in Eq. (A8) leads to

$$P^{(0)}_{yy}(q,i\omega) = -\frac{m^*\omega_p^2(q)d}{4\pi\hbar N_{2D}N}\int_0^{\hbar\beta} d\tau\ e^{i\omega\tau}\sum_s |\langle s|\hat{\beta}_y|0\rangle|^2\Big(e^{-E_s\tau/\hbar}\langle B_{s,q}B^\dagger_{s,q}\rangle_0 + e^{E_s\tau/\hbar}\langle B^\dagger_{s,-q}B_{s,-q}\rangle_0\Big). \tag{A11}$$

This can be easily integrated to give

$$P^{(0)}_{yy}(q,i\omega) = -\frac{m^*\omega_p^2(q)d}{4\pi\hbar N_{2D}N}\sum_s |\langle s|\hat{\beta}_y|0\rangle|^2\Big(\frac{e^{-\beta E_s}-1}{i\omega - E_s/\hbar}\langle B_{s,q}B^\dagger_{s,q}\rangle_0 + \frac{e^{\beta E_s}-1}{i\omega + E_s/\hbar}\langle B^\dagger_{s,-q}B_{s,-q}\rangle_0\Big) \tag{A12}$$

due to the constraint $i\omega = 2n\pi/\hbar\beta$ (n is an integer) on the Matsubara frequency for bosons [80,89], yielding $e^{i\omega\hbar\beta} = 1$. From Eq. (A12), using Eq. (A6), the boson commutation relations, and the fact that $E_s(q)$ is an even function of q, one finally arrives at Eq. (30).

APPENDIX B: PROOF OF EQ. (37)

For the *interacting* SWCN array, as per Eq. (A3), the positive-τ statistical averaging in Eq. (29) with the Heisenberg-picture dipole operators explicitly written is of the form

$$e^{\beta\Omega}\,\mathrm{Tr}\big[e^{-\beta(\hat{H}_0+\hat{H}_{\rm int})}T_\tau e^{\tau(\hat{H}_0+\hat{H}_{\rm int})}\hat{d}_y(q)e^{-\tau(\hat{H}_0+\hat{H}_{\rm int})}\hat{d}_y(-q)\big],$$
$$e^{-\beta\Omega} = \mathrm{Tr}\big[e^{-\beta(\hat{H}_0+\hat{H}_{\rm int})}\big].$$

This can be equivalently recast (see Ref. [80] for details) by writing all the operators in the interaction representation defined by Eq. (A9), to take the form

$$e^{\beta\Omega}\,\mathrm{Tr}\big[e^{-\beta\hat{H}_0}T_\tau S(\beta)\hat{d}_y(q,\tau)\hat{d}_y(-q,0)\big], \tag{B1}$$

with

$$e^{-\beta\Omega} = \mathrm{Tr}\big[e^{-\beta\hat{H}_0}S(\beta)\big], \tag{B2}$$

where $S(\beta)$ stands for the S matrix defined as follows:

$$S(\beta) = T_\tau\exp\Big[-\frac{1}{\hbar}\int_0^{\hbar\beta}d\tau\ \hat{H}_{\rm int}(\tau)\Big] = \sum_{n=0}^{\infty}\frac{(-1/\hbar)^n}{n!}\prod_{i,j=1}^{n}\int_0^{\hbar\beta}d\tau_i\ T_\tau\hat{H}_{\rm int}(\tau_j). \tag{B3}$$

The S-matrix series expansion, Eq. (B3), produces a series of summands in Eq. (B1), which after the τ-ordered operator pairings are done per Wick's theorem, can be classified in terms of the two types of Feynman diagrams. They are disconnected and connected diagrams (with and without "bubbles," respectively). More specifically [80], the $n \geq 1$ terms of Eq. (B3) generate in the exponential factor of Eq. (B2) the (vacuum polarization) disconnected diagrams of increasing order in $\hat{H}_{\rm int}(\tau_j)$, which cancel out exactly the disconnected diagrams of the trace expression in Eq. (B1). As a result, Eq. (B1) takes the form

$$e^{\beta\Omega_0}\,\mathrm{Tr}\big[e^{-\beta\hat{H}_0}T_\tau S(\beta)\hat{d}_y(q,\tau)\hat{d}_y(-q,0)\big] = \langle T_\tau S(\beta)\hat{d}_y(q,\tau)\hat{d}_y(-q,0)\rangle_0, \tag{B4}$$

with $\langle\cdots\rangle_0$ defined by Eqs. (A4) and (A5) where *only* the connected diagrams are to be retained and summed up. The interacting SWCN array polarization of Eq. (29) takes the form

$$P_{yy}(q,i\omega) = -\frac{1}{\hbar}\int_0^{\hbar\beta}d\tau\ e^{i\omega\tau}\langle T_\tau S(\beta)\hat{d}_y(q,\tau)\hat{d}_y(-q,0)\rangle_0, \tag{B5}$$

accordingly. Here, all the operators are written in the interaction representation defined by Eq. (A9) and the averaging with the S matrix of Eq. (B3) expands explicitly as follows:

$$\langle T_\tau S(\beta)\hat{d}_y(q,\tau)\hat{d}_y(-q,0)\rangle_0 = \sum_{n=0}^{\infty}\frac{(-1/\hbar)^n}{n!}\int_0^{\hbar\beta}d\tau_1\cdots\int_0^{\hbar\beta}d\tau_n\ \langle T_\tau\hat{d}_y(q,\tau)\hat{H}_{\rm int}(\tau_1)\cdots\hat{H}_{\rm int}(\tau_n)\hat{d}_y(-q,0)\rangle_0. \tag{B6}$$

Putting in here the perturbation $\hat{H}_{\rm int}$ in its explicit form, Eq. (16), brings the right-hand side of Eq. (B6) to the form

$$\sum_{n=0}^{\infty}\frac{(-1/\hbar)^n}{n!}\int_0^{\hbar\beta}d\tau_1\cdots\int_0^{\hbar\beta}d\tau_n\,\langle T_\tau\hat{d}_y(q,\tau)\frac{2\pi}{v_0}\sum_{q_1}\hat{d}_y(q_1,\tau_1)\hat{d}_y(-q_1,\tau_1)\cdots\frac{2\pi}{v_0}\sum_{q_n}\hat{d}_y(q_n,\tau_n)\hat{d}_y(-q_n,\tau_n)\hat{d}_y(-q,0)\rangle_0,$$

or more explicitly,

$$\langle T_\tau\hat{d}_y(q,\tau)\hat{d}_y(-q,0)\rangle_0-\frac{2\pi}{\hbar v_0}\sum_{q_1}\int_0^{\hbar\beta}d\tau_1\langle T_\tau\hat{d}_y(q,\tau)\hat{d}_y(q_1,\tau_1)\hat{d}_y(-q_1,\tau_1)\hat{d}_y(-q,0)\rangle_0$$

$$+\frac{1}{2}\Big(\frac{2\pi}{\hbar v_0}\Big)^2\sum_{q_1,q_2}\int_0^{\hbar\beta}d\tau_1\int_0^{\hbar\beta}d\tau_2\langle T_\tau\hat{d}_y(q,\tau)\hat{d}_y(q_1,\tau_1)\hat{d}_y(-q_1,\tau_1)\hat{d}_y(q_2,\tau_2)\hat{d}_y(-q_2,\tau_2)\hat{d}_y(-q,0)\rangle_0-\cdots.$$

This, after the pairing of the induced dipole operators per Wick's theorem with *only* the connected Feynman diagram terms retained, gives

$$\langle T_\tau S(\beta)\hat{d}_y(q,\tau)\hat{d}_y(-q,0)\rangle_0=\langle T_\tau\hat{d}_y(q,\tau)\hat{d}_y(-q,0)\rangle_0-\int_0^{\hbar\beta}d\tau_1\langle T_\tau\hat{d}_y(q,\tau)\hat{d}_y(-q,\tau_1)\rangle_0\frac{2\pi}{\hbar v_0}\,\langle T_\tau\hat{d}_y(q,\tau_1)\hat{d}_y(-q,0)\rangle_0$$

$$+\int_0^{\hbar\beta}d\tau_1\int_0^{\hbar\beta}d\tau_2\langle T_\tau\hat{d}_y(q,\tau)\hat{d}_y(-q,\tau_1)\rangle_0\frac{2\pi}{\hbar v_0}\,\langle T_\tau\hat{d}_y(q,\tau_1)\hat{d}_y(-q,\tau_2)\rangle_0\frac{2\pi}{\hbar v_0}\,\langle T_\tau\hat{d}_y(q,\tau_2)\hat{d}_y(-q,0)\rangle_0-\cdots. \tag{B7}$$

In here, it is reflected that *only* the summands with $q_1=q_2=\cdots=q$ produced by the pairing as shown can contribute nonzero trace values for the trace taken over the complete set of states, Eq. (A2), of the noninteracting exciton Hilbert space. Substituting Eq. (B7) in Eq. (B5) and using the Matsubara (complex-time) function Fourier transform properties for bosons (see Ref. [80]), summarized in our case as follows:

$$P_{yy}(q,i\omega)=\int_0^{\hbar\beta}d\tau\;e^{i\omega\tau}P^{(0)}_{yy}(q,\tau),$$

$$\omega=\omega_n=\frac{2\pi n}{\hbar\beta},n=0,\pm1,\pm2,\ldots,$$

$$P^{(0)}_{yy}(q,\tau-\tau')=\frac{1}{\hbar\beta}\sum_{\omega_n}e^{-i\omega_n(\tau-\tau')}P^{(0)}_{yy}(q,i\omega_n),$$

$$\frac{1}{\hbar\beta}\int_0^{\hbar\beta}d\tau\;e^{i(\omega_n-\omega_{n'})\tau}=\delta_{\omega_n\omega_{n'}},$$

$$\frac{1}{\hbar\beta}\sum_{\omega_n}e^{-i\omega_n(\tau-\tau')}=\delta(\tau-\tau'),$$

one obtains an infinite series

$$P_{yy}(q,i\omega)=P^{(0)}_{yy}(q,i\omega)+P^{(0)}_{yy}(q,i\omega)\frac{2\pi}{v_0}P^{(0)}_{yy}(q,i\omega)$$

$$+P^{(0)}_{yy}(q,i\omega)\frac{2\pi}{v_0}P^{(0)}_{yy}(q,i\omega)\frac{2\pi}{v_0}P^{(0)}_{yy}(q,i\omega)+\cdots,$$

which can be rewritten in the closed form

$$P_{yy}(q,i\omega)=P^{(0)}_{yy}(q,i\omega)+P^{(0)}_{yy}(q,i\omega)\frac{2\pi}{v_0}P_{yy}(q,i\omega)$$

that results in Eq. (37).

[1] M. Dresselhaus, G. Dresselhaus, and Ph. Avouris, eds. *Carbon Nanotubes: Synthesis, Structure, Properties, and Applications* (Springer-Verlag, Berlin, 2001).

[2] S. M. Huang, B. Maynor, X. Y. Cai, and J. Liu, Ultra-long, well-aligned single-walled carbon nanotube architectures on surfaces, Adv. Mater. **15**, 1651 (2003).

[3] L. X. Zheng, M. J. O'Connell, S. K. Doorn, X. Z. Liao, Y. H. Zhao, E. A. Akhadov, M. A. Hoffbauer, B. J. Roop, Q. X. Jia, R. C. Dye, D. E. Peterson, S. M. Huang, J. Liu, and Y. T. Zhu, Ultralong single-wall carbon nanotubes, Nat. Mater. **3**, 673 (2004).

[4] M. F. L. De Volder, S. H. Tawfick, R. H. Baughman, and A. J. Hart, Carbon nanotubes: Present and future commercial applications, Science **339**, 535 (2013).

[5] K. Tsukagoshi, B. W. Alphenaar, and H. Ago, Coherent transport of electron spin in a ferromagnetically contacted carbon nanotube, Nature **401**, 572 (1999).

[6] C. W. Chang, D. Okawa, A. Majumdar, and A. Zettl, Solid-state thermal rectifier, Science **314**, 1121 (2006).

[7] Ph. Avouris, M. Freitag, and V. Perebeinos, Carbon-nanotube photonics and optoelectronics, Nat. Photon. **2**, 341 (2008).

[8] T. Hertel, Carbon nanotubes: A brighter future, Nat. Photon. **4**, 77 (2010).

[9] I. V. Bondarev, Surface electromagnetic phenomena in pristine and atomically doped carbon nanotubes, J. Comp. Theor. Nanosci. **7**, 1673 (2010).

[10] I. V. Bondarev, M. F. Gelin, and A. V. Meliksetyan, in *Dekker Encyclopedia of Nanoscience and Nanotechnology* (CRC Press: New York, 2014), 3rd ed., p. 4989.

[11] S. Cambré, J. Campo, C. Beirnaert, C. Verlackt, P. Cool, and W. Wenseleers, Asymmetric dyes align inside carbon nanotubes to yield a large nonlinear optical response, Nat. Nanotechn. **10**, 248 (2015).

[12] X. Ma, N. F. Hartmann, J. K. S. Baldwin, S. K. Doorn, and H. Htoon, Room-temperature single-photon generation from solitary dopants of carbon nanotubes, Nat. Nanotechn. **10**, 671 (2015).

[13] F. Pyatkov, V. Fütterling, S. Khasminskaya, B. S. Flavel, F. Hennrich, M. M. Kappes, R. Krupke, and W. H. P. Pernice, Cavity-enhanced light emission from electrically driven carbon nanotubes, Nat. Photon. **10**, 420 (2016).

[14] M.-Y. Wu, J. Zhao, N. J. Curley, T.-H. Chang, Z. Ma, and M. S. Arnold, Biaxially stretchable carbon nanotube transistors, J. Appl. Phys. **122**, 124901 (2017).

[15] J.-H. Han, G. L. Paulus, R. Maruyama, D. A. Heller, W.-J. Kim, P. W. Barone, C. Y. Lee, J. H. Choi, M.-H. Ham, C. Song, C. Fantini, and M. S. Strano, Exciton antennas and concentrators from core-shell and corrugated carbon nanotube filaments of homogeneous composition, Nat. Mater. **9**, 833 (2010).

[16] I. Robel, B. A. Bunker, and P. V. Kamat, SWCNT-CdS nanocomposite as light harvesting assembly. Photoinduced charge transfer interactions, Adv. Mater. **17**, 2458 (2005).

[17] F. Vietmeyer, B. Seger, and P. V. Kamat, Anchoring ZnO particles on functionalized single wall carbon nanotubes. Excited state interactions and charge collection, Adv. Mater. **19**, 2935 (2007).

[18] S. D. Stranks, C. Weisspfennig, P. Parkinson, M. B. Johnston, L. M. Herz, and R. J. Nicholas, Ultrafast charge separation at a polymer-single-walled carbon nanotube molecular junction, Nano Lett. **11**, 66 (2011).

[19] X. Dang, H. Yi, M.-H. Ham, J. Qi, D. S. Yun, R. Ladewski, M. S. Strano, P. T. Hammond, and A. M. Belcher, Virus-templated self-assembled single-walled carbon nanotubes for highly efficient electron collection in photovoltaic devices, Nat. Nanotechn. **6**, 377 (2011).

[20] I. V. Bondarev and B. Vlahovic, Optical absorption by atomically doped carbon nanotubes, Phys. Rev. B **74**, 073401 (2006).

[21] S. Berciaud, L. Cognet, P. Poulin, R. B. Weisman, and B. Lounis, Absorption spectroscopy of individual single-walled carbon nanotubes, Nano Lett. **7**, 1203 (2007).

[22] J.-C. Blancon, M. Paillet, H. N. Tran, X. T. Than, S. A. Guebrou, A. Ayari, A. S. Miguel, N.-M. Phan, A.-A. Zahab, J.-L. Sauvajol, N. D. Fatti, and F. Vallée, Direct measurement of the absolute absorption spectrum of individual semiconducting single-wall carbon nanotubes, Nat. Commun. **4**, 2542 (2013).

[23] A. Roch, L. Stepien, T. Roch, I. Dani, C. Leyens, O. Jost, and A. Leson, Optical absorption spectroscopy and properties of single walled carbon nanotubes at high temperature, Synth. Met. **197**, 182 (2014).

[24] I. V. Bondarev, Plasmon enhanced raman scattering effect for an atom near a carbon nanotube, Opt. Express **23**, 3971 (2015).

[25] A. G. Marinopoulos, L. Reining, A. Rubio, and N. Vast, Optical and Loss Spectra of Carbon Nanotubes: Depolarization Effects and Intertube Interactions, Phys. Rev. Lett. **91**, 046402 (2003).

[26] F. S. Hage, T. P. Hardcastle, A. J. Scott, R. Brydson, and Q. M. Ramasse, Momentum- and space-resolved high-resolution electron energy loss spectroscopy of individual single-wall carbon nanotubes, Phys. Rev. B **95**, 195411 (2017).

[27] M. F. Gelin and I. V. Bondarev, One-dimensional transport in hybrid metal-semiconductor nanotube systems, Phys. Rev. B **93**, 115422 (2016).

[28] T. Ando, Theory of electronic states and transport in carbon nanotubes, J. Phys. Soc. Jpn. **74**, 777 (2005).

[29] M. S. Dresselhaus, G. Dresselhaus, R. Saito, and A. Jorio, Exciton photophysics of carbon nanotubes, Annu. Rev. Phys. Chem. **58**, 719 (2007).

[30] I. V. Bondarev, L. M. Woods, and K. Tatur, Strong exciton-plasmon coupling in semiconducting carbon nanotubes, Phys. Rev. B **80**, 085407 (2009).

[31] T. Ando, Environment effects on excitons in semiconducting carbon nanotubes, J. Phys. Soc. Jpn. **79**, 024706 (2010).

[32] I. V. Bondarev, Asymptotic exchange coupling of quasi-one-dimensional excitons in carbon nanotubes, Phys. Rev. B **83**, 153409 (2011).

[33] I. V. Bondarev and T. Antonijevic, Surface plasmon amplification under controlled exciton-plasmon coupling in individual carbon nanotubes, Phys. Status Solidi C **9**, 1259 (2012).

[34] I. V. Bondarev, Single-wall carbon nanotubes as coherent plasmon generators, Phys. Rev. B **85**, 035448 (2012).

[35] Q. Zhang, E. H. Hároz, Z. Jin, L. Ren, X. Wang, R. S. Arvidson, A. Lüttge, and J. Kono, Plasmonic nature of the terahertz conductivity peak in single-wall carbon nanotubes, Nano Lett. **13**, 5991 (2013).

[36] I. V. Bondarev and A. V. Meliksetyan, Possibility for exciton bose-einstein condensation in carbon nanotubes, Phys. Rev. B **89**, 045414 (2014).

[37] I. V. Bondarev, Relative stability of excitonic complexes in quasi-one-dimensional semiconductors, Phys. Rev. B **90**, 245430 (2014).

[38] T. Morimoto, S.-K. Joung, T. Saito, D. N. Futaba, K. Hata, and T. Okazaki, Length-dependent plasmon resonance in single-walled carbon nanotubes, ACS Nano **8**, 9897 (2014).

[39] L. Martín-Moreno, F. J. Garcïa de Abajo, and F. J. Garcïa-Vidal, Ultraefficient coupling of a quantum emitter to the tunable guided plasmons of a carbon nanotube, Phys. Rev. Lett **115**, 173601 (2015).

[40] A. Graf, L. Tropf, Y. Zakharko, J. Zaumseil, and M. C. Gather, Near-infrared exciton-polaritons in strongly coupled single-walled carbon nanotube microcavities, Nat. Commun. **7**, 13078 (2016).

[41] I. V. Bondarev and A. Popescu, Exciton bose-einstein condensation in double walled carbon nanotubes, MRS Adv. **2**, 2401 (2017).

[42] A. S. Kadochkin, S. G. Moiseev, Y. S. Dadoenkova, V. V. Svetukhin, and I. O. Zolotovskii, Surface plasmon polariton amplification in a single-walled carbon nanotube, Opt. Express **25**, 27165 (2017).

[43] W. Gao, X. Li, M. Bamba, and J. Kono, Continuous transition between weak and ultrastrong coupling through exceptional points in carbon nanotube microcavity exciton-polaritons, Nat. Phot. **12**, 362 (2018).

[44] T. Hertel and I. V. Bondarev, Photophysics of carbon nanotubes and nanotube composites, Chem. Phys. **413**, 1 (2013), (Special Issue, T. Hertel, I.V. Bondarev, Eds.)

[45] X. He, W. Gao, L. Xie, B. Li, Q. Zhang, S. Lei, J. M. Robinson, E. H. Hároz, S. K. Doorn, W. Wang, R Vajtai, P. M. Ajayan, W. W. Adams, R. H. Hauge, and J. Kono, Wafer-scale monodomain films of spontaneously aligned single-walled carbon nanotubes, Nat. Nanotechn. **11**, 633 (2016).

[46] A. L. Falk, K.-C. Chiu, D. B. Farmer, Q. Cao, J. Tersoff, and Y.-H. Lee, Coherent Plasmon and Phonon-Plasmon Resonances in Carbon Nanotubes, Phys. Rev. Lett. **118**, 257401 (2017).

[47] K.-C. Chiu, A. L. Falk, P.-H. Ho, D. B. Farmer, G. Tulevski, Y.-H. Lee, P. Avouris, and S.-J. Han, Strong and broadly tunable plasmon resonances in thick films of aligned carbon nanotubes, Nano Lett. **17**, 5641 (2017).

[48] P.-H. Ho, D. B. Farmer, G. S. Tulevski, S.-J. Han, D. M. Bishop, L. M. Gignac, J. Bucchignano, Ph. Avouris, and A. L. Falk, Intrinsically ultrastrong plasmon-exciton interactions in crystallized films of carbon nanotubes, PNAS **115**, 12662 (2018).

[49] M. E. Green, D. A. Bas, H.-Y. Yao, J. J. Gengler, R. J. Headrick, T. C. Back, A. M. Urbas, M. Pasquali, J. Kono, and T.-H. Her, Bright and ultrafast photoelectron emission from aligned single-wall carbon nanotubes through multiphoton exciton resonance, Nano Lett. **19**, 158 (2019).

[50] W. Gao, C. F. Doiron, X. Li, J. Kono, and G. V. Naik, Macroscopically aligned carbon nanotubes as a refractory platform for hyperbolic thermal emitters, ACS Photonics **6**, 1602 (2019).

[51] J. A. Roberts, S.-J. Yu, P.-H. Ho, S. Schoeche, A. L. Falk, and J. A. Fan, Tunable hyperbolic metamaterials based on self-assembled carbon nanotubes, Nano Lett. **19**, 3131 (2019).

[52] S. Schöche, P.-H. Ho, J. A. Roberts, S. J. Yu, J. A. Fan, and A. L. Falk, Mid-IR and UV-Vis-NIR mueller matrix ellipsometry characterization of tunable hyperbolic metamaterials based on self-assembled carbon nanotubes, J. Vac. Sci. Technol. B **38**, 014015 (2020).

[53] N. Komatsu, M. Nakamura, S. Ghosh, D. Kim, H. Chen, A. Katagiri, Y. Yomogida, W. Gao, K. Yanagi, and J. Kono, Groove-assisted global spontaneous alignment of carbon nanotubes in vacuum filtration, Nano Lett. **20**, 2332 (2020).

[54] J. A. Roberts, P.-H. Ho, S.-J. Yu, X. Wu, Y. Luo, W. L. Wilson, A. L. Falk, and J. A. Fan, Multiple Tunable Hyperbolic Resonances in Broadband Infrared Carbon-Nanotube Metamaterials, Phys. Rev. Appl. **14**, 044006 (2020).

[55] I. V. Bondarev, H. Mousavi, and V. M. Shalaev, Transdimensional epsilon-near-zero modes in planar plasmonic nanostructures, Phys. Rev. Res. **2**, 013070 (2020).

[56] I. V. Bondarev, Finite-thickness effects in plasmonic films with periodic cylindrical anisotropy [Invited], Opt. Mater. Express **9**, 285 (2019).

[57] I. V. Bondarev, H. Mousavi, and V. M. Shalaev, Optical response of finite-thickness ultrathin plasmonic films, MRS Commun. **8**, 1092 (2018).

[58] I. V. Bondarev and V. M. Shalaev, Universal features of the optical properties of ultrathin plasmonic films, Opt. Mater. Express **7**, 3731 (2017).

[59] A. Boltasseva and V. M. Shalaev, Transdimensional photonics, ACS Photon. **6**, 1 (2019).

[60] I. V. Bondarev and Ph. Lambin, Spontaneous-decay dynamics in atomically doped carbon nanotubes, Phys. Rev. B **70**, 035407 (2004).

[61] F. J. Garsia-Vidal, J. M. Pitarke, and J. B. Pendry, Effective Medium Theory of the Optical Properties of Aligned Carbon Nanotubes, Phys. Rev. Lett. **78**, 4289 (1997).

[62] J. M. Pitarke, F. J. Garsia-Vidal, and J. B. Pendry, Effective electronic response of a system of metallic cylinders, Phys. Rev. B **57**, 15261 (1998).

[63] F. J. Garsia-Vidal, J. M. Pitarke, and J. B. Pendry, Silver-filled nanotubes used as spectroscopic enhancers, Phys. Rev. B **58**, 6783 (1998).

[64] Z. M. Li, Z. K. Tang, H. J. Liu, N. Wang, C. T. Chan, R. Saito, S. Okada, G. D. Li, J. S. Chen, N. Nagasawa, and S. Tsuda, Polarized Absorption Spectra of Single-Walled 4Å Carbon Nanotubes Aligned in Channels of an $AlPO_4 - 5$ Single Crystal, Phys. Rev. Lett. **87**, 127401 (2001).

[65] D. R. Smith and D. Schurig, Electromagnetic Wave Propagation in Media with Indefinite Permittivity and Permeability Tensors, Phys. Rev. Lett. **90**, 077405 (2003).

[66] W. Cai and V. Shalaev, *Optical Metamaterials: Fundamentals & Applications* (Springer-Verlag, New York, 2010).

[67] N. I. Zheludev and Y. S. Kivshar, From metamaterials to metadevices, Nat. Mater. **11**, 917 (2012).

[68] A. V. Kildishev, A. Boltasseva, and V. M. Shalaev, Planar photonics with metasurfaces, Science **339**, 1289 (2013).

[69] K. V. Sreekanth, Y. Alapan, M. E. Kabbash, E. Ilker, M. Hinczewski, U. A. Gurkan, A. D. Luca, and G. Strangi, Extreme sensitivity biosensing platform based on hyperbolic metamaterials, Nat. Mater. **15**, 621 (2016).

[70] N. I. Landy, S. Sajuyigbe, J. J. Mock, D. R. Smith, and W. J. Padilla, Perfect Metamaterial Absorber, Phys. Rev. Lett. **100**, 207402 (2008).

[71] J. B. Pendry, D. Schurig, and D. R. Smith, Controlling electromagnetic fields, Science **312**, 1780 (2006).

[72] Z. Liu, H. Lee, Y. Xiong, C. Sun, and X. Zhang, Far-field optical hyperlens magnifying sub-diffraction-limited objects, Science **315**, 1686 (2007).

[73] I. V. Bondarev and A. V. Gulyuk, Electromagnetic SERS effect in carbon nanotube systems, Superlatt. Microstr. **87**, 103 (2015).
[74] M. F. Gelin, I. V. Bondarev, and A. V. Meliksetyan, Optically promoted bipartite atomic entanglement in hybrid metallic carbon nanotube systems, J. Chem. Phys. **140**, 064301 (2014).
[75] M. F. Gelin, I. V. Bondarev, and A. V. Meliksetyan, Monitoring bipartite entanglement in hybrid carbon nanotube systems via optical 2D photon-echo spectroscopy, Chem. Phys. **413**, 123 (2013).
[76] J. Galego, F. J. Garcia-Vidal, and J. Feist, Cavity-Induced Modifications of Molecular Structure in the Strong-Coupling Regime, Phys. Rev. X **5**, 041022 (2015).
[77] J. Galego, F. J. Garcia-Vidal, and J. Feist, Suppressing photochemical reactions with quantized light fields, Nat. Commun. **7**, 13841 (2016).
[78] I. V. Bondarev and Ph. Lambin, van der waals coupling in atomically doped carbon nanotubes, Phys. Rev. B **72**, 035451 (2005).
[79] I. V. Bondarev and Ph. Lambin, in *Trends in Nanotubes Research* (Nova Publishers, New York, 2006), Ch. 6, p. 139.
[80] G. D. Mahan, *Many-Particle Physics* (Kluwer Academic, New York, 2000), 3rd ed.
[81] V. A. Markel, Introduction to the Maxwell garnett approximation: Tutorial, J. Opt. Soc. Am. A **33**, 1244 (2016).
[82] L. V. Keldysh, Coulomb interaction in thin semiconductor and semimetal films, Pis'ma Zh. Eksp. Teor. Fiz. **29**, 716 (1979), [Engl. translation: JETP. Lett. **29**, 658 (1980)].
[83] J. Deslippe, M. Dipoppa, D. Prendergast, M. V. O. Moutinho, R. B. Capaz, and S. G. Louie, Electron-hole interaction in carbon nanotubes: Novel screening and exciton excitation spectra, Nano Lett. **9**, 1330 (2009).
[84] L. X. Benedict, S. G. Louie, and M. L. Cohen, Static polarizabilities of single-wall carbon nanotubes, Phys. Rev. B **52**, 8541 (1995).
[85] B. Kozinsky and N. Marzari, Static Dielectric Properties of Carbon Nanotubes from First Principles, Phys. Rev. Lett. **96**, 166801 (2006).
[86] S. Tasaki, K. Maekawa, and T. Yamabe, π-band contribution to the optical properties of carbon nanotubes: Effects of chirality, Phys. Rev. B **57**, 9301 (1998).
[87] H. Haken, *Quantum Field Theory of Solids* (North-Holland, Amsterdam, 1976).
[88] N. N. Bogolubov and N. N. Bogolubov Jr., *Introduction to Quantum Statistical Mechanics* (World Scientific, Singapore, 2010), 2nd ed.
[89] A. Abrikosov, L. Gor'kov, and I. Dzyaloshinski, *Methods of Quantum Field Theory in Statistical Physicsl* (Dover Publication, New York, 1975).
[90] T. Nakanishi and T. Ando, Optical response of finite-length carbon nanotubes, J. Phys. Soc. Jpn. **78**, 114708 (2009).
[91] V. Perebeinos and Ph. Avouris, Exciton ionization, Franz-Keldysh, and Stark Effects in carbon nanotubes, Nano Lett. **7**, 609 (2007).
[92] L. Vertchenko, L. Leandro, E. Shkondin, O. Takayama, I. V. Bondarev, N. Akopian, and A. V. Lavrinenko, Cryogenic characterization of titanium nitride thin films, Opt. Mater. Express **9**, 2117 (2019).
[93] P. Y. Yu and M. Cardona, *Fundamentals of Semiconductors. Physics and Material Properties* (Springer, Heidelberg, 2010).
[94] Z. Guo, H. Jiang, and H. Chena, Hyperbolic metamaterials: From dispersion manipulation to applications, J. Appl. Phys. **127**, 071101 (2020).
[95] L. D. Landau and E. M. Lifshitz, *Statistical Physics* (Pergamon, Oxford, 1980).
[96] E. S. Abers, *Quantum Mechanics* (Pearson, NJ, 2004).